Mon. Not. R. Astron. Soc. **382,** 1552–1590 (2007) doi:10.1111/j.1365-2966.2007.12006.x

Multiwavelength study of the nuclei of a volume-limited sample of galaxies – II. Optical, infrared and radio observations

P. Lira,[1⋆] R. A. Johnson,[2] A. Lawrence[3] and R. Cid Fernandes[4]

[1]*Departamento de Astronomía, Universidad de Chile, Casilla 36-D, Santiago, Chile*
[2]*Astrophysics, Oxford University, Denys Wilkinson Building, Keble Road, Oxford OX1 3RH*
[3]*SUPA*[1]†*, Institute for Astronomy, University of Edinburgh, Royal Observatory, Blackford Hill, Edinburgh EH9 3HJ*
[4]*Departamento de de Física – CFM – Universidade Federal de Santa Catarina, Florianópolis, SC, Brazil*

Accepted 2007 May 15. Received 2007 April 10; in original form 2006 December 19

ABSTRACT

We present optical and infrared broad-band images, radio maps, and optical spectroscopy for the nuclear region of a sample of nearby galaxies. The galaxies have been drawn from a complete volume-limited sample for which we have already presented X-ray imaging. We modelled the stellar component of the spectroscopic observations to determine the star formation history of our targets. Diagnostic diagrams were used to classify the emission-line spectra and determine the ionizing mechanism driving the nuclear regions. All those sources classified as active galactic nuclei present small Eddington ratios ($\sim 10^{-3}$–10^{-6}), implying a very slow growth rate of their black holes. We finally investigate the relative numbers of active and normal nuclei as a function of host galaxy luminosity and find that the fraction of active galaxies slowly rises as a function of host absolute magnitude in the $M_B \sim -12$ to -22 range.

Key words: galaxies: active – galaxies: general – galaxies: nuclei.

1 INTRODUCTION

This is the second paper studying the nuclear properties of a volume-limited sample of galaxies. The sample contains galaxies from the KKT catalogue (Kraan-Korteweg & Tamman 1979; Kraan-Korteweg 1986) within a distance of 7.6 Mpc, brighter than $M_B \sim -13$, with $\delta > -35^\circ$ and either with a Hubble type of Sd or earlier, or classified as a blue compact dwarf. This gives a basic sample of 37 nearby galaxies containing the nearest examples of various morphological types and a representative range of intrinsic luminosities. Since the sample was defined updated distances have become available for many of these galaxies and are used throughout this paper. The new distances, galaxy celestial coordinates,[1] morphology (or Hubble Type), and absolute magnitudes corrected for foreground extinction (Schlegel, Finkbeiner & Davis 1998) are listed in Table 1.

The main goals of the survey are to investigate how common low-luminosity active nuclei are and how this activity is connected with the host galaxy properties. To address these issues, we have collected multiwavelength images of the galaxies and follow up with moderate-to-high signal-to-noise ratio (S/N) spectroscopy of a list of nuclear candidate 'hotspots'.

In Paper I (Lira, Lawrence & Johnson 2000), we presented the results from *ROSAT* HRI X-ray imaging of 33 of the galaxies in the sample. The main results were that weak ($L_X \gtrsim 10^{38}$ erg s^{-1}) nuclear X-ray sources were found to be very common, with a detection rate of ∼35 per cent, and that the probability of detecting a nuclear source increases with host luminosity.

In this paper, we will present CCD imaging of the sample in the optical (*UBVRI*) and infrared (IR) (*JHK*), radio observations, and optical spectroscopy for multiple locations in the nuclear regions. Section 2 describes the acquisition and reduction of the data. Section 3 presents an atlas of the observations while Section 4 gives details of the data analysis. The characteristics of the stellar component are presented in Section 5. A discussion based on the results from line-emission diagnostic diagrams is given in Section 6. Finally, Section 7 looks at the demographics of active galactic nuclei (AGN) and their relationship with host galaxy luminosities.

2 OBSERVATIONS AND DATA REDUCTION

2.1 Broad-band observations

Broad-band optical images of the galaxies were obtained at the 1-m Jacobus Kapteyn Telescope in La Palma in 1994 February and August. The *UBVRI* images had a pixel scale of ∼0.3 arcsec and the total field of view (FOV) was of ∼6 arcmin. Near-infrared (NIR) images were taken at the 2.1-m telescope of the Observatorio Astronómico Nacional in Baja California in 1994 October and 1995

⋆E-mail: plira@das.uchile.cl
†Scottish Universities Physics Alliance.

[1]Note that in Paper I (Lira, Lawrence & Johnson 2000) the coordinates given in table 1 correspond to B1950, not to J2000.

Table 1. The volume-limited sample of galaxies. Revised distances and references are given.

Galaxy	RA (J2000)	Dec. (J2000)	M_B^0	Hubble type	Distribution (Mpc)	Reference	Galaxy	RA (J2000)	Dec. (J2000)	M_B^0	Hubble type	Distribution (Mpc)	Reference
NGC 147	00:33:12	+48:30:30	−14.5	dE5	0.68	M05	NGC 3738	11:35:48	+54:31:28	−16.6	Sd	4.9	K03a
NGC 185	00:38:58	+48:20:12	−14.7	dE3	0.62	M05	NGC 4136	12:09:18	+29:55:39	−17.7	Sc	6.94	K79
NGC 205	00:40:22	+41:41:26	−16.1	S0/E5	0.82	M05	NGC 4144	12:09:59	+46:27:27	−17.3	Scd	7.45	S05
NGC 221	00:42:42	+40:51:52	−16.0	E2	0.78[a]		NGC 4150	12:10:33	+30:24:05	−18.5	S0/a	14.4	R05
NGC 224	00:42:44	+41:16:09	−20.5	Sb	0.78	M05	NGC 4236	12:16:43	+69:27:56	−18.2	SBd	4.45	K02
NGC 247	00:47:08	−20:45:38	−17.5	Sc	2.88	D02	NGC 4244	12:17:30	+37:48:29	−17.7	Scd	4.5	K03a
NGC 253	00:47:33	−25:17:18	−20.1	Sc	3.94	K03c	UGC 7321	12:17:35	+22:32:23	−16.3	Scd	10[b]	U03
NGC 404	01:09:27	+35:43:03	−16.7	S0	3.42	Ti03	NGC 4395	12:25:50	+33:32:27	−17.6	Sd	4.3	T04
NGC 598	01:33:59	+30:39:37	−18.6	Sc	0.84	F01	NGC 4605	12:40:00	+61:36:32	−17.3	Sc	4.26	B02
MAFFEI 1	02:36:21	+59:38:51	−18.7	E3	3.01	F03	NGC 4736	12:50:53	+41:07:12	−19.7	RSab	4.7	K03b
MAFFEI 2	02:41:55	+59:36:15	−22.0	Sbc	2.8	K03d	NGC 4826	12:56:44	+21:41:05	−19.5	Sab	5	R94
IC 342	03:46:50	+68:05:45	−20.5	Scd	3.3	S02	NGC 5204	13:29:37	+58:25:04	−16.6	Sd	4.6	K03b
NGC 1560	04:32:51	+71:53:20	−16.6	Sd	3.45	K03d	NGC 5238	13:37:01	−29:51:58	−15.1	Sdm	5.2	M98
NGC 2366	07:28:52	+69:12:34	−16.0	SBm	3.19	K03a	NGC 5236	13:34:43	+51:36:49	−20.3	SBc	4.5	Th03
NGC 2403	07:36:55	+65:35:58	−18.9	Sc	3.22	F01	NGC 5457	14:03:13	+54:21:02	−21.0	Sc	6.7	F01
NGC 2976	09:47:17	+67:54:51	−17.0	Sd	3.56	K04	NGC 6503	17:49:28	+70:08:41	−17.7	Sc	5.27	K03b
A 0951+68	09:57:08	+68:35:54	−12.8	dE	3.60	K04	NGC 6946	20:34:52	+60:09:14	−20.7	Sc	5.9	S97
NGC 3031	09:55:33	+69:03:55	−20.4	Sb	3.63	F01	NGC 7793	23:57:50	−32:35:21	−18.3	Sd	3.91	K03c
UGC 6456	11:28:01	+78:59:35	−14.1	Peculiar	4.42	M02							

[a]M 32 is assumed to be at the same distance as M 31. [b]Distance very uncertain, in the range 7–13 Mpc.

References. M05: McConnachie et al. (2005), D02: Davidge & Courteau (2002), K03b: Karachentsev et al. (2003b), Ti03: Tikhonov et al. (2003), F01: Freedman et al. (2001), F03: Fingerhut et al. (2003), K03d: Karachentsev et al. (2003d), S02: Saha et al. (2002), K03a: Karachentsev et al. (2003a), K04: Karachentsev et al. (2004), M02: Méndez et al. (2002), K79: Kraan-Korteweg & Tamman (1979), S05: Seth et al. (2005), R05: Rekola et al. (2005), K02: Karachentsev et al. (2002), U03: Uson & Matthews (2003), T04: Thim et al. (2004), B02: Bolatto et al. (2002), K03b:Karachentsev et al. (2003b), R94: Rubin (1994), M98: Makarova & Karachentsev (1998), Th03: Thim et al. (2003), S97: Sharina et al. (1997), and K03c: Karachentsev et al. (2003c).

March and October. *JHK* images were obtained with a pixel scale of ∼0.5 arcsec and an FOV of ∼2 arcmin.

Radio observations at 1.4 GHz were taken with the Very Large Array (VLA) in B configuration in 1994 August. These are supplemented with radio data from the literature and from the VLA FIRST catalogue (Becker, White & Helfand 1995).

Both the optical and NIR data were reduced using the IRAF software. The optical data were debiased and flat-fielded, and calibrated using Landolt standard stars (Landolt 1983, 1992). The NIR data were sky-subtracted and flat-fielded. No flux calibration was obtained for these images. Cleaned images were produced from our radio data using AIPS. The pixel size for the radio images was chosen to be 1 arcsec.

Table 2 gives the detected flux or upper limit of radio sources found in the nuclear regions. Sources with spectroscopic observations are noted in the last column of the table. Both the FIRST and our own VLA measurements correspond to integrated fluxes derived by fitting an elliptical Gaussian model to the central source (White et al. 1997).

2.2 Optical spectroscopy

From the broad-band NIR, radio, optical, and X-ray images presented here and in Paper I, targets in the nuclear regions of the galaxies were selected for long-slit spectroscopy with the William Herschel Telescope (WHT). While some galaxies had a distinctive nucleus, detected at several different wavelengths, others had multiple 'hotspots', possibly appearing in different wavelength bands, with no single, well-defined, unique nucleus. We targeted those sources that were conspicuous in any of the multiwavelength images and located in the nuclear region of the galaxies. As can be seen in Section 3, these sources were all found in the inner few hundred parsecs of the galaxies.

For the acquisition of optically faint targets, or radio sources without optical counterparts (MAFFEI 2-2, MAFFEI 2-3, NGC 4826-2 and NGC 4826-3; see Table 2), the observations were done in 'blind-offset' mode from a reference star. X-ray sources without optical counterparts were not followed up since the absolute accuracy in the *ROSAT* X-ray positions is ∼5 arcsec (Paper I).

Long-slit spectra of the nuclear targets were obtained on 1996 July 13–15 and 1997 January 15 using the 4.2-m WHT at the Observatorio Roque de los Muchachos. Table 3 shows a summary of set-ups. The slit width was 1 arcsec with the seeing varying between ∼0.8 and ∼1.2 arcsec during both runs. The slit was positioned at the parallactic angle to minimize light losses. During the run of 1996 July no clouds were present, although the presence of Saharan dust in the atmosphere hampered the observations. The conditions during 1997 January were not photometric. Therefore, no absolute flux calibration was determined for the observations. An example spectrum is shown in Fig. 1.

The data were reduced using IRAF software. Standard reduction procedures (bias subtraction, flat-fielding, slit illumination correction) were applied. The extraction of the galactic spectra was achieved using an extraction window of width ∼2.2 arcsec. The wavelength calibration was performed using comparison copper–neon and copper–argon lamps. Badly subtracted skylines were removed from the spectra by hand using the IRAF package SPLOT.

The spectra have been corrected for foreground extinction as tabulated by Schlegel et al. (1998) using the empirical extinction function of Cardelli, Clayton & Mathis (1989).

A comparison of relative emission-line fluxes common to this work and the survey published by Ho, Filippenko & Sargent (1997a) shows a good agreement between both sets of data, with differences of typically less than 20 per cent for lines from HIIR-dominated spectra (e.g. NGC 1560, NGC 2976, NGC 3738 and NGC 6946). Therefore relative fluxes for our spectra are considered reliable.

Some data showed calibration problems in the region of overlap between the red and blue spectra. These are due to poor fitting of the rapid decline in sensitivity near the dichroic crossover point and at the short-wavelength end of the blue arm, probably due to uncertainties in the wavelength calibration. However, the mismatches were present in only ∼5 per cent of the spectra.

3 GALAXY ATLAS

Fig. 2 shows the images of galaxies in our sample ordered with increasing right ascension. Source celestial coordinates can be found in Table 1. For all the galaxies with the necessary JKT data, we provide broad-band optical (usually *R*) images of the whole galaxy (unless the galaxy is larger than our FOV) and of the central regions (usually 1 × 1 kpc, except for very nearby galaxies). The dashed box on the large image shows the area displayed in the image of the central regions. The scale bar on the large image always denotes 30 arcmin, and that on the central region image always denotes 10 arcmin.

For some galaxies we also show a colour image. In the colour images, the lighter regions are bluer. We only show NIR images for a few galaxies where the NIR provides additional information (e.g. a clear identification of the nucleus).

For galaxies without JKT data we searched for images in public archives and data bases. Table 4 gives the source of each image.

For the galaxies where central radio sources were detected in our own data or in the FIRST survey, we have overlaid the radio data as contour maps on the broad-band optical images. For galaxies with central radio sources found in the literature, we have marked the radio positions on the JKT images with the crosses.

Spectra from sources in the nuclear region of the galaxies in our sample are also shown in Fig. 2. Although fluxes are given on an absolute scale, it must be remembered that the observations were not taken under photometric conditions. All spectra have been corrected for foreground extinction (Schlegel et al. 1998).

For galaxies with more than one nuclear target, several spectra were acquired. The names of the spectra correspond to the labels given in the optical images. When galaxies had an obvious nucleus with no other candidates for spectroscopy, a single spectrum is shown.

Notes on selected objects can be found in Appendix A.

4 DATA ANALYSIS

4.1 Imaging analysis

The *optical* images in Fig. 2 show that several galaxies – NGC 253, MAFFEI 2, IC 342, NGC 2403, NGC 2976, UGC 6456, NGC 3738, NGC 4144, NGC 4236, NGC 5204, NGC 5238, NGC 5236, NGC 5457 and NGC 6946 – contain central regions which are patchy, that is, they have uneven central surface brightnesses with the presence of several bright sources which can be considered as candidate nuclei.

These galaxies are all late-type spirals, with morphological types of Sc or later. Knapen et al. (2006) found patchy Hα emission in the central regions of late-type spirals. This is consistent with our colour images which indicate that a mixture of star formation and dust extinction is responsible for the patchy appearance of these galaxies.

Table 2. Nuclear radio sources. Upper limits correspond to 5σ values, unless otherwise noted. The last column indicates those sources that had spectroscopic follow-up, the name of the spectrum shown in Fig. 2, and whether the radio sources are coincident with the galaxy nucleus (N).

Galaxy	RA (J2000)	Dec. (J2000)	Flux in mJy (wavelength)	Reference	Atlas
NGC 147			<1.47 (21 cm)	VLA	
NGC 185			<1.1 (10σ at 2 cm)	N00	
NGC 205			<2.0 (21 cm)	VLA	
NGC 221			<1.32 (21 cm)	VLA	
			<0.03 (2 cm) <0.53 (6 cm) <0.55 (21 cm)	H03	
NGC 224	0:42:42.33	41:16:08.4	0.028 (3.6 cm)	C92	NGC 224 (N)
NGC 247			<3.83 (21 cm)	VLA	
NGC 253	0:47:33.17	−25:17:17.0	35.79 (1.3 cm) 40.32 (2 cm)	U97	NGC 253 (N)
	”	”	47.95 (3.6 cm) 38.64 (6 cm)	U97	”
NGC 404	1:09:27.01	35:43:04.8	2.88 (21 cm)	VLA	NGC 404 (N)
			<10 (0.7 cm) <1.3 (2 cm) <0.9 (3.6 cm)	N00	
NGC 598	1:33:50.67	30:41:19.9	0.2 (6 cm) 0.6 (20 cm)[a]	G99	NGC 598 (N)
MAFFEI 1	2:36:35.21	59:39:22.4	4.24 (21 cm)	VLA	
MAFFEI 2	2:41:55.08	59:36:14.1	4.0 (6 cm)[b] 1.9 (2 cm)[b]	T94	
	2:41:55.08	59:36:16.0	5.6 (6 cm)[b] 2.1 (2 cm)[b]	T94	MAFFEI 2-2
	2:41:55.12	59:36:17.8	6.2 (6 cm)[b] 2.3 (2 cm)[b]	T94	
	2:41:55.09	59:36:21.3	4.7 (6 cm)[b] 2.4 (2 cm)[b]	T94	MAFFEI 2-3
IC 342	3:46:48.41	68:05:47.9	2.3 (6 cm)[c]	T83	IC 342-1 (N)
NGC 1560			<1.05 (21 cm)	VLA	
NGC 2366			<5.45	Hu01	
NGC 2403			< 0.22 (6 cm)	T94	
NGC 2976			<1.03 (21 cm)	VLA	
			<0.047 (6 cm)	U02	
A 0951+68			<1.63 (21 cm)	VLA	
NGC 3031	9:55:33.18	69:03:55.0	118 ± 6, 121 ± 6 (1.3 cm) 118 ± 8 (3.6 cm)	B96	No follow-up (N)
	”	”	120 (2 cm) 160 (3.6 cm) 140 (6 cm) 100 (20 cm)	H99	”
	”	”	164.8 (2 cm)	N02	”
	”	”	127 (3.6 cm)[d]	B00	”
NGC 3738			<0.94 (20 cm)	FIRST	
NGC 4136			<0.95 (20 cm)	FIRST	
			<0.1 (6 cm)	U02	
NGC 4144			<0.93 (20 cm)	FIRST	
NGC 4150			<0.93 (20 cm)	FIRST	
			<1.0 (2 cm)	N02	
NGC 4236			<0.22 (6 cm)	T94	
NGC 4244			<1.37 (20 cm)	FIRST	
UGC 7321			<0.94 (20 cm)	FIRST	
NGC 4395	12:25:48.87	33:32:48.7	1.17 (20 cm)	FIRST	NGC 4395 (N)
	”	”	0.8 (6 cm) 1.68 (20 cm)	H01	”
	”	”	0.530 (VLBA,20 cm)	W01	”
NGC 4605			<0.5	U02	
NGC 4736	12:50:53.02	41:08:13.2	13.51 (20 cm)	FIRST	NGC 4736 (N)
	”	”	6.1 (6 cm), 3.2 (2 cm)	T94	”
	”	”	1.7 (2 cm)	N02	”
NGC 4826	12:56:43.64	21:40:59.1	36.06 (20 cm)	FIRST	NGC 4826-1 (N)
	”	”	1.4 (6 cm)[b] 0.6 (2 cm)[b]	T94	”
	12:56:43.39	21:41:00.1	1.7 (6 cm)[b] 0.5 (2 cm)[b]	T94	
	12:56:43.40	21:40:58.7	0.7 (6 cm)[b] 0.8 (2 cm)[b]	T94	
	12:56:43.91	21:40:58.0	0.4 (6 cm)[b] 0.5 (2 cm)[b]	T94	NGC 4826-2
	12:56:43.63	21:41:02.9	1.1 (6 cm)[b] 0.4 (2 cm)[b]	T94	NGC 4826-3
NGC 5238			<0.97 (20 cm)	FIRST	
NGC 5236	13:37:00.93	−29:51:54.61	≈1 (6 cm)[e]	T94	No follow-up (N)
NGC 5457	14:03:12.39	54:20:54.5	3 (6 cm)[c]	T94	NGC 5457-1 (N)
			<0.93 (20 cm)	FIRST	
NGC 6503			<1.0 (2 cm)	N02	
NGC 6946	20:34:52.3	60:09:14.5	6 (6 cm)[c]	T83	NGC 6946 (N)

[a]Total flux; unclear if source is compact or extended. [b]Extended source, peak flux. [c]Extended source; no dominant peak; total flux. [d]Mean value – strongly variable. [e]Estimate of peak flux at an optical nucleus.

References. N00: Nagar et al. (2000), H03: Ho, Terashima & Ulvestad (2003), C92: Crane, Dickel & Cowan (1992), U97: Ulvestad & Antonucci (1997), G99: Gordon et al. (1999), T94: Turner & Ho (1994), T83: Turner & Ho (1983), Hu01: Hunter, Elmegreen & vanWoerden (2001), U02: Ulvestad & Ho (2002), B96: Bietenholz et al. (1996), H99: Ho et al. (1999), N02: Nagar et al. (2002), B00: Bietenholz, Bartel & Rupen (2000), H01: Ho & Ulvestad (2001), W01: Wrobel, Fassnacht & Ho (2001).

Table 3. Set-up for spectroscopy.

	1996 July		1997 January	
	Blue	Red	Blue	Red
CCD	LORAL	Tek	Tek	Tek
Grating	R300B	R316R	R300B	R316R
λ range (Å)	3538–5460	5312–6807	3655–5223	5270-6765
Resolution (Å)	∼3.8	∼3.0	∼3.5	∼3.0
Dispersion (Å pixel^{-1})	0.96	1.47	1.54	1.47
Scale (arcsec pixel^{-1})	0.22	0.36	0.36	0.36

In fact, for NGC 253, MAFFEI 2, IC 342, NGC 2403, NGC 5204, NGC 5236, NGC 5457 and NGC 6946 a true nucleus can be identified from observations at other wavelengths obtained by us and found in the literature (see Appendix A for details), leaving 6/37 galaxies which have ambiguous nuclei.

NGC 2366 is classified as a peculiar galaxy and does not seem to have a single candidate nucleus in the optical images. In contrast with the previous group, this galaxy presents a rather smooth and flat central surface brightness. We have examined the nature of two bright knots of emission (see Appendix A) to find that they correspond to a foreground star and an off-centre cluster.

Late-type spirals with no obvious nucleus have been found by Böker et al. (2002) in their search for nuclear star clusters in 77 spirals of morphological type Scd–Sm using optical imaging. They found that ≈23 per cent of the galaxies in their sample contained no nuclear cluster. All galaxies in our sample with no or ambiguous nuclei have types Scd or later (including NGC 2366, and excluding the dE galaxies NGC 147 and NGC 185 – see below). They represent a large fraction of the total number of late spirals (13), giving a fraction of 7/13 (≈54 per cent). This is probably a luminosity effect since Böker's sample does not include galaxies with $M_B^0 \gtrsim -16.5$. If we apply this restriction to our sample, the fraction of late spirals without an obvious nucleus becomes comparable (4/13 ≈31 per cent).

Note that NGC 6946 is in both our sample and Böker's, but Böker fails to find a nuclear cluster in this object due to the presence of the large amount of dust present in the nuclear region. In our NIR images, nuclear regions generally appear much more symmetric than in the optical (see Fig. 2), showing the effects of dust. For NGC 6946, the brightest sources seen in the optical and NIR images are coincident, leading us to conclude that NGC 6946 does have an obvious nucleus (see also Elmegreen, Chromey & Warren 1998).

Two dwarf ellipticals in our sample – NGC 147 and NGC 185 – have several bright knots in their central regions. We have examined the nature of these sources (see Appendix A) and found that for NGC 147 they correspond to foreground stars and a globular cluster, while for NGC 185 no single source presents particular characteristics to recognise it as the true nucleus. In fact, dEs often do not show the presence of a nucleus, and the ratio of nucleated to non-nucleated dEs decreases with decreasing luminosity (Ferguson & Binggeli 1994).

4.2 Radio analysis

Two early-type galaxies, NGC 404 (S0) and MAFFEI 1 (E3), have nuclear radio sources detected in our VLA data. The source in NGC 404 is marginally extended, with a 21-cm flux of 2.88 mJy, and the source in MAFFEI 1 is compact with a 21-cm flux of 4.24 mJy. Using the distances in Table 1 gives 21-cm luminosities of 4.03×10^{18} WHz^{-1} in NGC 404 and 4.60×10^{18} WHz^{-1} in MAFFEI 1. These luminosities are at the low end of the radio luminosities seen in nearby early-type galaxies (Wrobel & Heeschen 1991).

Of the galaxies in our sample with data from the FIRST survey, three spirals, NGC 4395, NGC 4736 and NGC 4826, have detected nuclear sources. Again using the distances from Table 1, the 21-cm nuclear source luminosities in NGC 4395, NGC 4736 and NGC 4826 are 2.59×10^{18} WHz^{-1}, 3.57×10^{19} and 1.08×10^{20} WHz^{-1}, respectively.

NGC 4395 is a well-known dwarf Seyfert galaxy and is one of only two nuclear intermediate-mass black holes that have been detected in the radio regime (Greene, Ho & Ulvestad 2006). The FIRST detection is consistent with previous detections (Ho & Ulvestad 2001; Wrobel et al. 2001; Wrobel & Ho 2006b) where the compactness, high brightness temperature and subparsec elongated emission of the central radio source all point to its being powered by accretion on to the black hole.

The extended central radio sources in NGC 4736 and NGC 4826 are both likely caused by star-forming regions and/or supernova remnants (SNRs) from central star formation.

4.3 Spectral analysis

The first step in the spectral analysis was to study the stellar component using the STARLIGHT spectral synthesis code developed by Cid

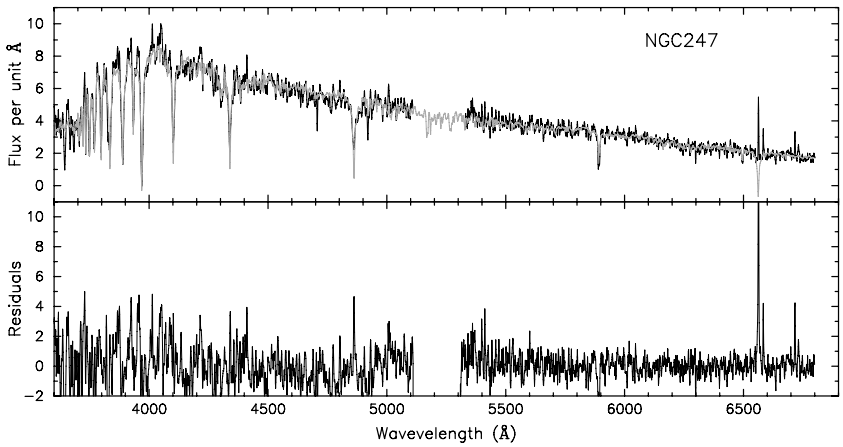

Figure 1. Observed (black) and synthetic (grey) spectra for NGC 247. The bottom panel shows the residuals after subtracting the synthetic spectrum from the observations revealing a weak Hβ line.

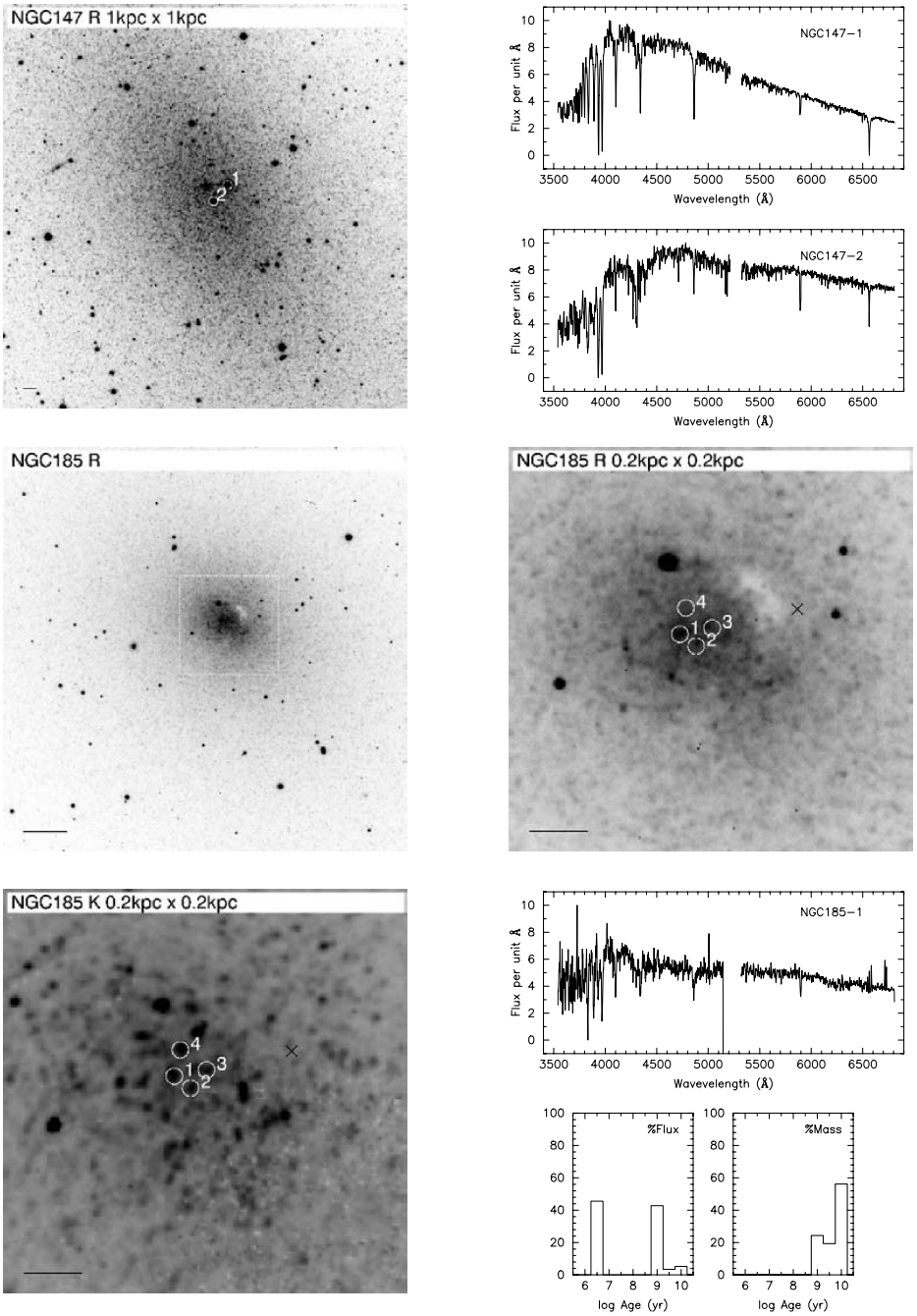

Figure 2. Imaging and spectroscopic atlas of the volume-limited sample of galaxies. A spectroscopic absolute flux calibration is not available. Results from the stellar population synthesis are also shown. For most galaxies we show broad-band images of the whole galaxy and an image of the central region (usually $1 \times 1\,\mathrm{kpc}^2$ – corresponding to the dashed box on the large images). The scale bar in the large image always denotes 30 arcmin, and that on the central region image always denotes 10 arcmin. For some galaxies, we also show a colour image where lighter regions are bluer. For the galaxies where central radio sources were detected in the VLT or FIRST data, we have overlaid radio contour maps. For galaxies with central radio sources in the literature, we have marked the radio positions with crosses. Notes on individual galaxy images: IC 342: the positions of the three central radio peaks (crosses) were measured from Turner & Ho (1983) by hand. NGC 5236: the radio source positions from Turner & Ho (1994) were shifted to correctly align the radio and optical sources (Gallais et al. 1991).

Fernandes et al. (2004, 2005), which takes advantage of the high spectral resolution library published by Bruzual & Charlot (2003). For the analysis, 45 different stellar population templates were used spanning ages between $\sim 10^6$ and 10^{10} yr, and metallicities $Z = 0.2 \times Z_\odot$, $Z_\odot$ and $2.5 \times Z_\odot$. The best-fitting spectrum is determined from χ^2-minimizing techniques after masking out all emission lines from the spectra.

Bad fits were caused by poor-S/N data, the calibration problem in the overlap region between the red and blue sides of the spectra (which in some cases was masked out during the fitting), and

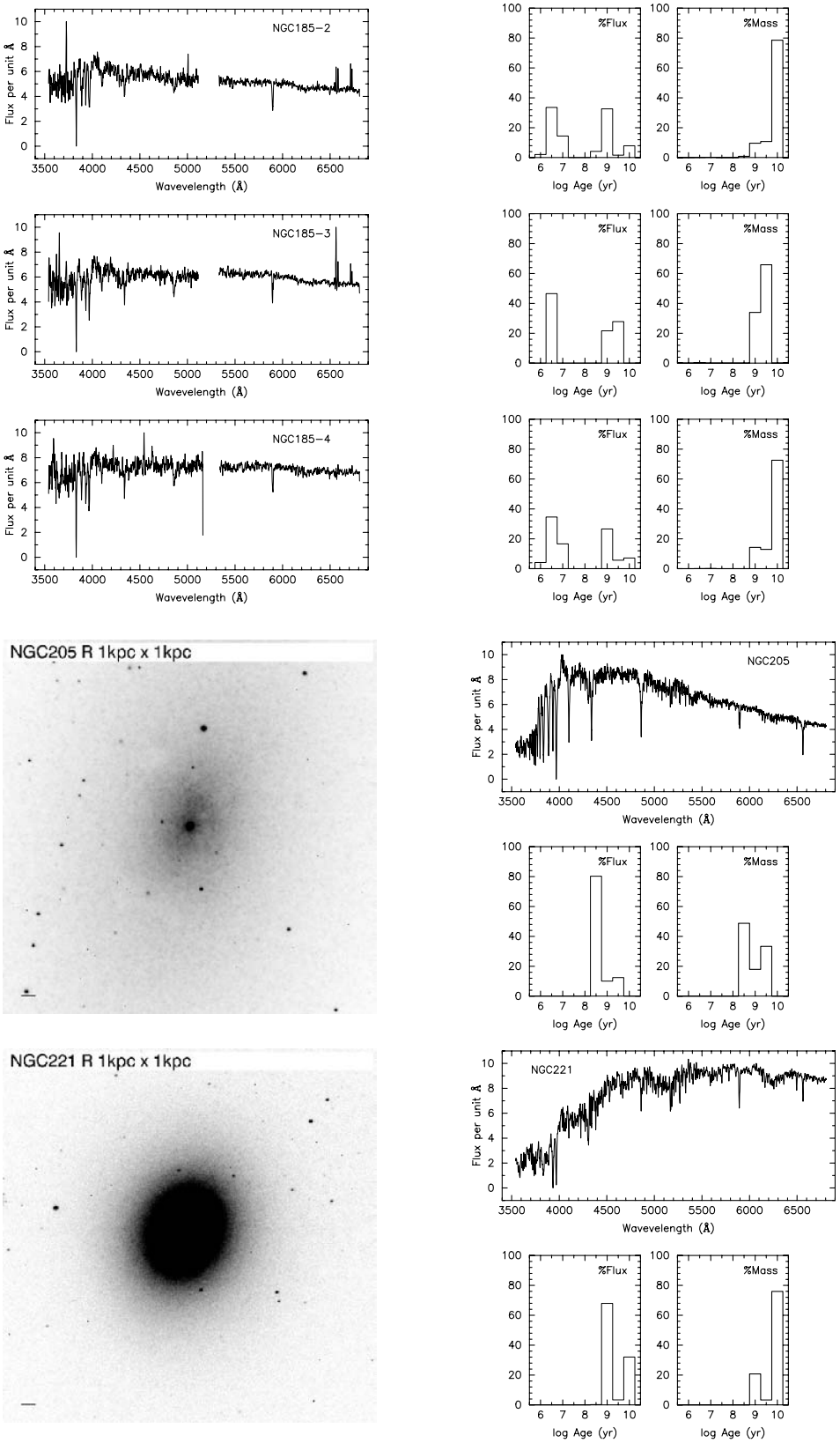

Figure 2 – *continued*

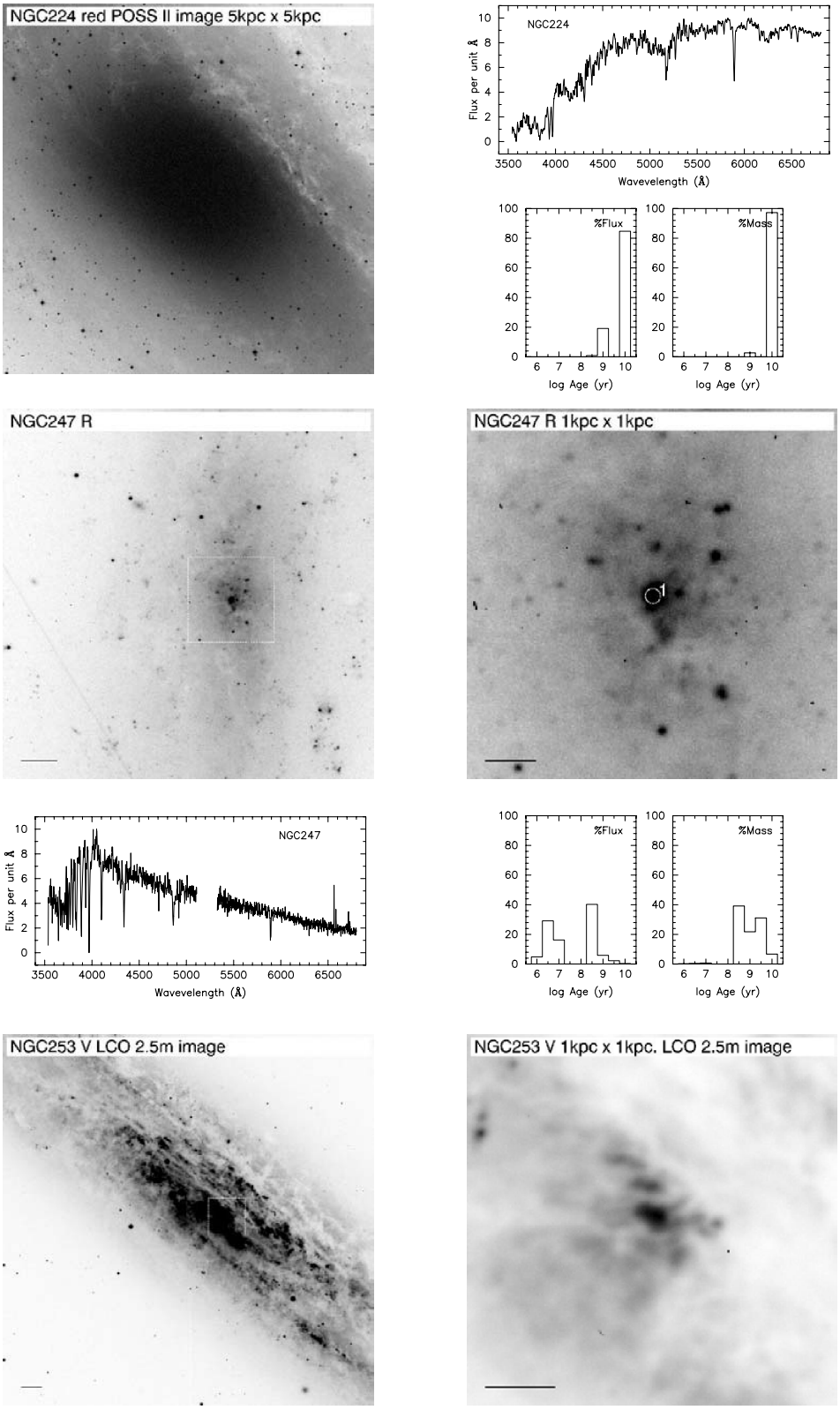

Figure 2 – *continued*

the lack of α-enriched templates in the code data base. From the code output it is possible to recover the flux, mass and enrichment history of the targets, as well as the intrinsic extinction and the velocity dispersion of the stellar component. For those spectra that had acceptable fits, we have included the flux distribution (i.e. the fraction of the flux at 4020 Å coming from stellar populations of different ages) and mass distribution (ditto) in the $\sim 10^6$–10^{10} yr age range. The masses take into account the deposition of material back

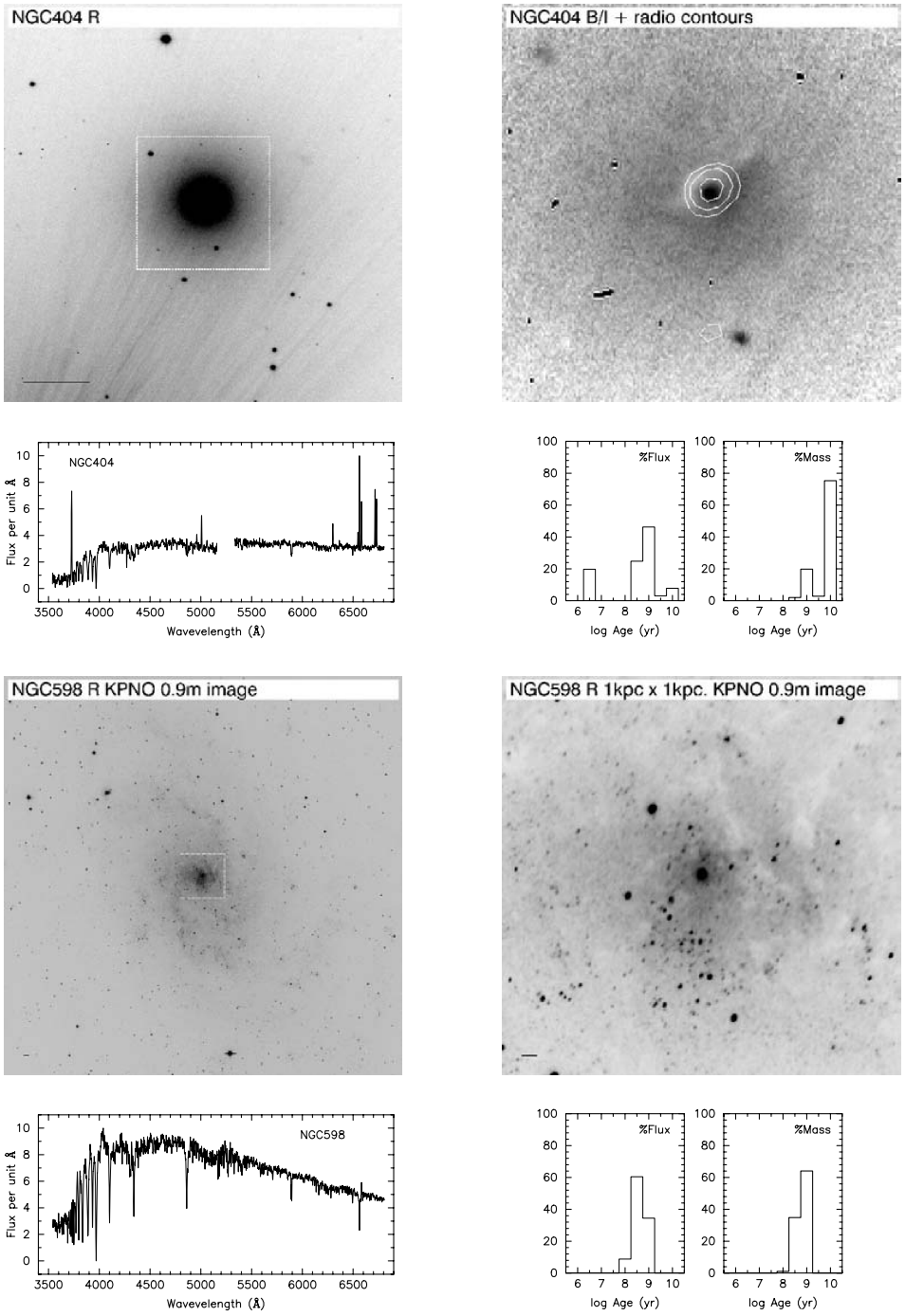

Figure 2 – *continued*

into the galactic interstellar medium (ISM) during stellar evolution and therefore correspond to the amount of material currently locked into stars.

The best-fitting models were then subtracted from the observed data to give pure emission-line spectra. This reveals weak emission lines present in targets with significant intermediate-age stellar populations. An example can be seen in Fig. 1. Emission-line fluxes were measured from the subtracted data using the IRAF package SPLOT and are presented in Table 6. To assess the errors associated with the line flux values, Gaussian profiles were fitted to lines from spectra with high and low S/Ns. The measurements were repeated for multiple observations of the same target. The measured Hα flux values for HIIR-like, high-S/N spectra (e.g. NGC 4605) showed scatter of less than 1 per cent, while the flux values for spectra with low S/N (e.g. NGC 185-2) showed scatter of 10–20 per cent. However, the largest source of uncertainty is associated with the process of subtraction of the stellar component, which might introduce substantial systematic errors. In Table 6, we have labelled those flux measurements with the largest uncertainties, estimated to be in the $\pm$50–100 per cent range.

Extinction estimations were derived from both, the population synthesis analysis of the stellar component, and the nebular

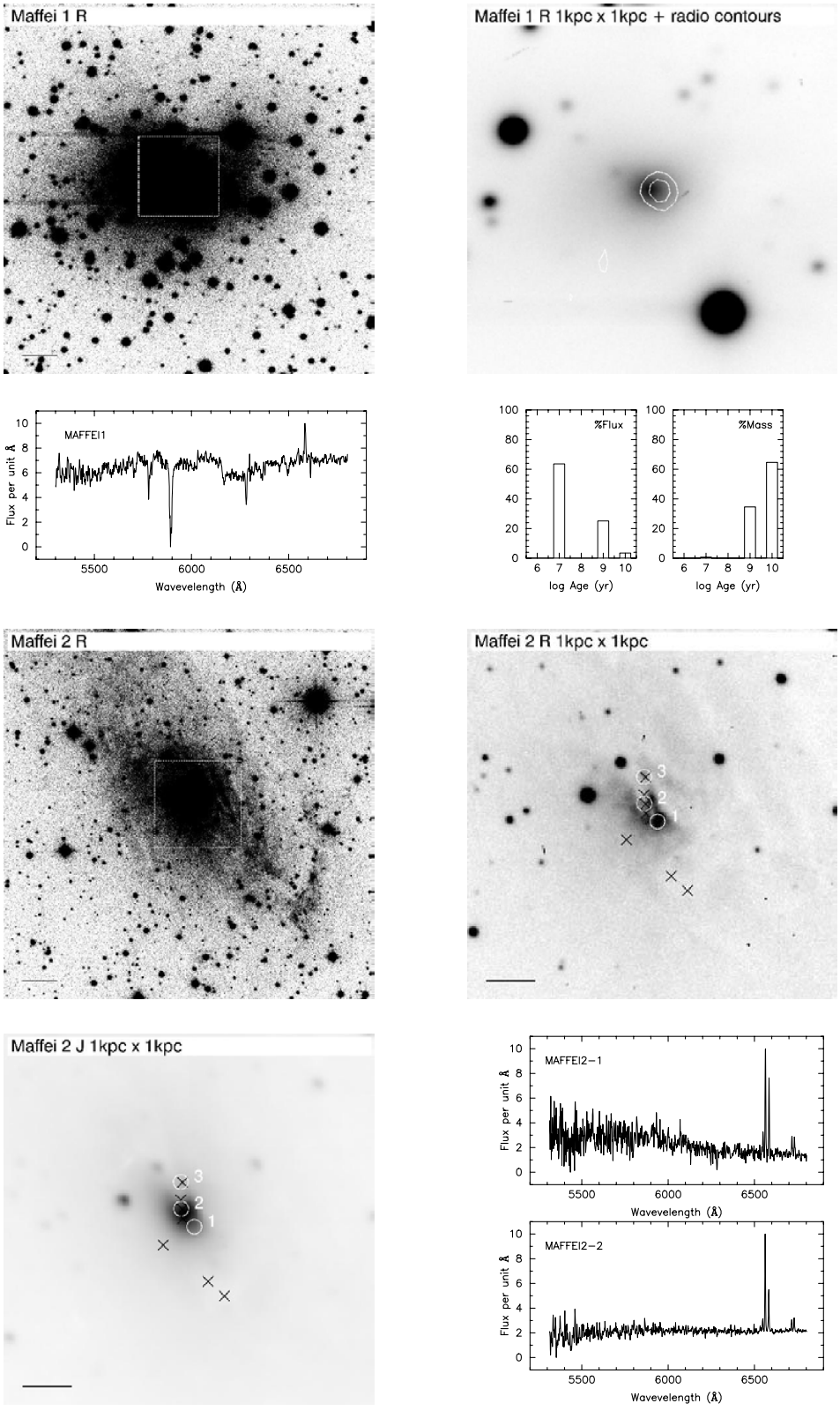

Figure 2 – *continued*

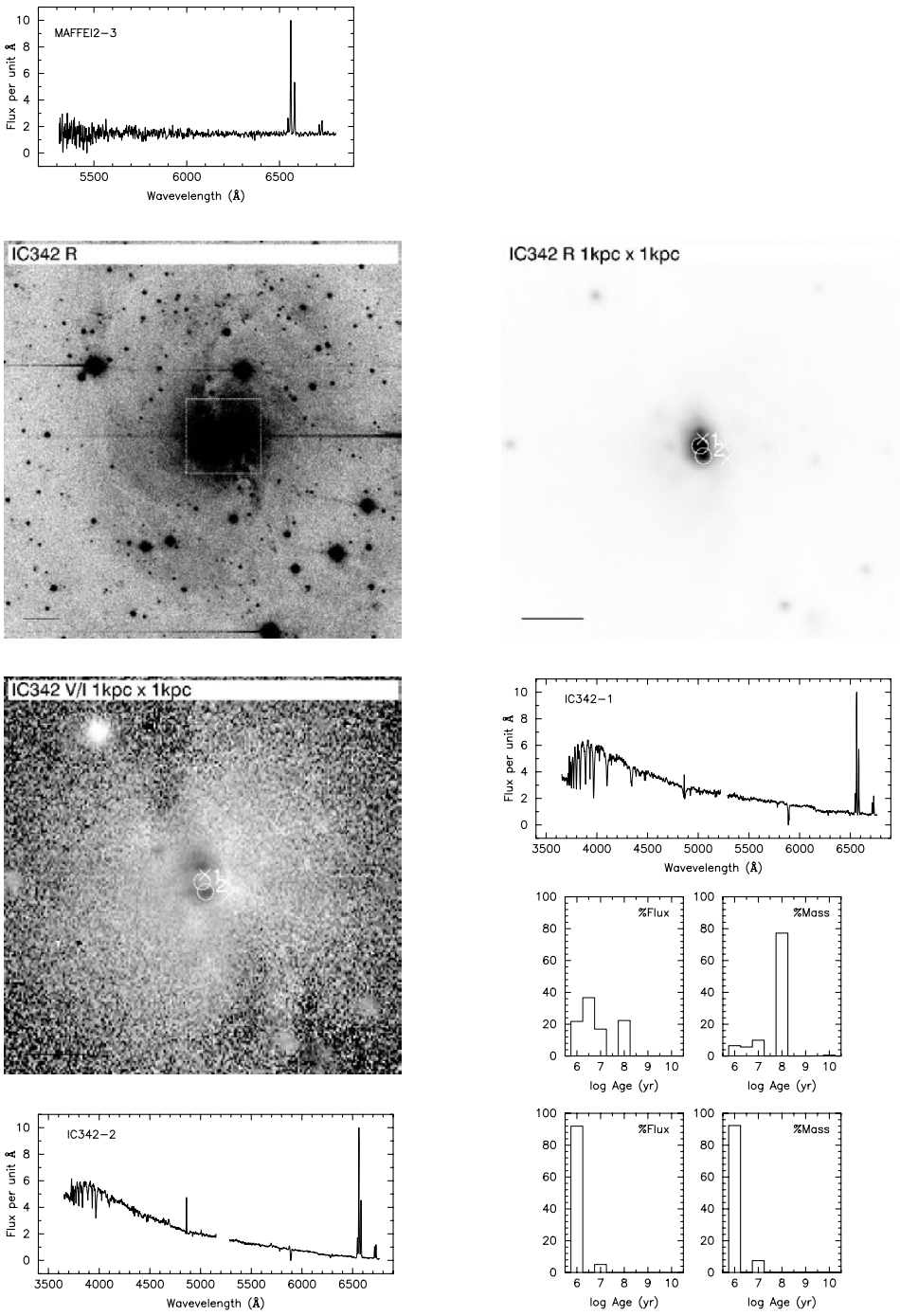

Figure 2 – *continued*

component derived assuming an $A_V(\mathrm{Neb}) = 7.35 \times \log([\mathrm{H}\alpha/\mathrm{H}\beta]/2.8)$, where $\mathrm{H}\alpha/\mathrm{H}\beta$ represents the line flux ratio. The results are shown in Table 7.

5 STELLAR AND GAS PROPERTIES

5.1 Star formation histories

Following Cid Fernandes et al. (2004, 2005) we have grouped the results from the population-synthesis analysis of our spectra in three age groups: a young component ($t < 10^8$ yr), an intermediate component ($10^8 < t < 10^9$ yr), and an old component ($t > 2.5 \times 10^9$ yr). The results are expected to have a ∼10 per cent accuracy (Cid Fernandes et al. 2004).

Table 8 shows the results in terms of percentage flux at 4020 Å and percentage mass for each age component. It is clear that galaxies show a wide range of star formation histories in their central regions. Note that while the starlight from all age groups is required to reproduce most of the observed spectra, the stellar masses correspond mostly to the intermediate and old populations. Because of the choice of reference wavelength for the contributed flux (4020 Å), the results present several cases where a young stellar

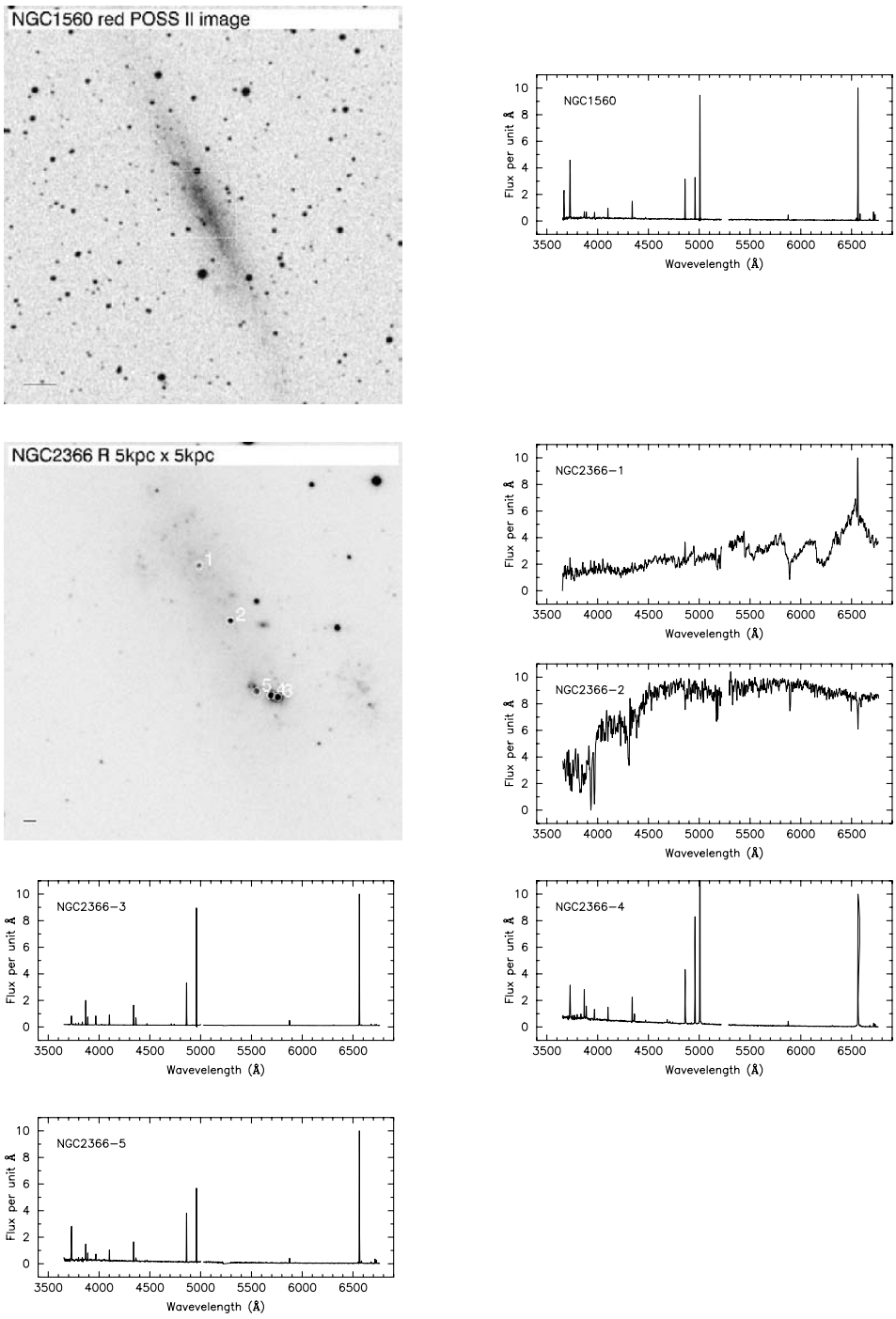

Figure 2 – *continued*

population has a negligible mass contribution (<1 per cent) but dominates the flux output at 4020 Å. Note also that stellar masses are determined assuming a mass-to-light ratio for each stellar component and are subject to significant uncertainties.

We have examined whether there is a correlation between the characteristics of the stellar populations and other galaxy properties, such as Hubble type, galaxy absolute magnitude, and the nuclear or off-nuclear nature of the sources. In Table 9, we show the percentage flux and mass as a function of age and metallicity.

Despite the small number of observed objects, Table 9 shows that sources in late-type galaxies are the only ones gathering a significant fraction of stellar mass (up to ∼10 per cent) in the last 100 Myr. It is also seen that dwarf galaxies are currently forming more stars than more massive galaxies. Since our targets for the spectroscopic follow-up were selected as nuclear 'hotspots' detected in the X-ray, optical, IR, and radio wavelengths, we are sampling the most actively star-forming regions in the these galaxies and therefore our results should be representative of the overall star formation in these nuclear regions.

Results on metallicity trends are very sketchy. In fact, accurate metallicity determinations are always problematic in population synthesis. The age–metallicity degeneracy can limit the amount of

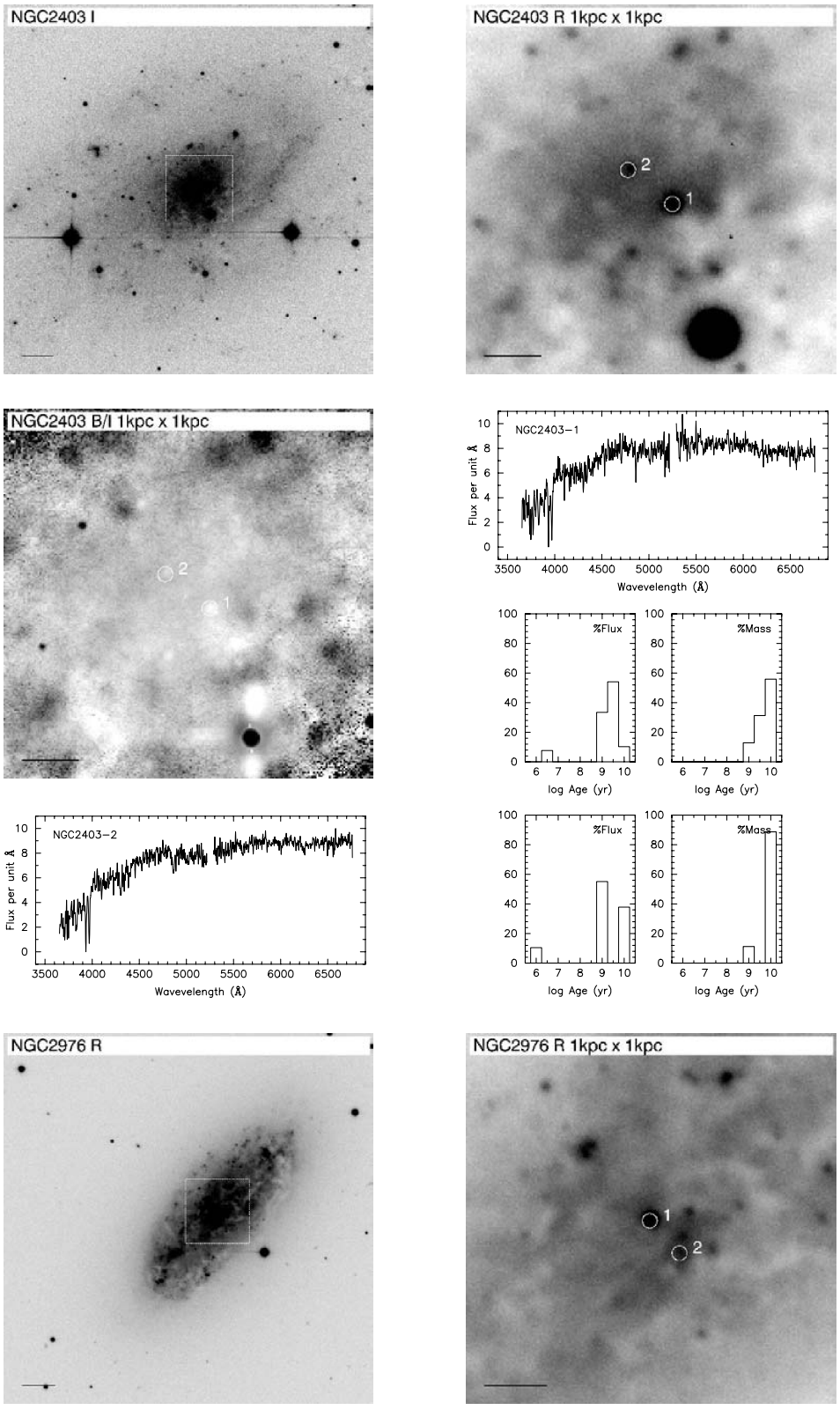

Figure 2 – *continued*

information which can be extracted from galaxy spectra. Furthermore, although the Padova evolutionary tracks used by Bruzual & Charlot (2003) are computed for $2.5\,Z_{\odot}$, the stellar library used to construct the synthetic spectrum does *not* contain stars this metal rich. Similar inconsistencies happen at lower metallicities (Bruzual & Charlot 2003). Hence, $2.5\,Z_{\odot}$ should be regarded as something just slightly over solar, the exact value being hard to define, given the inconsistencies between tracks and spectral libraries.

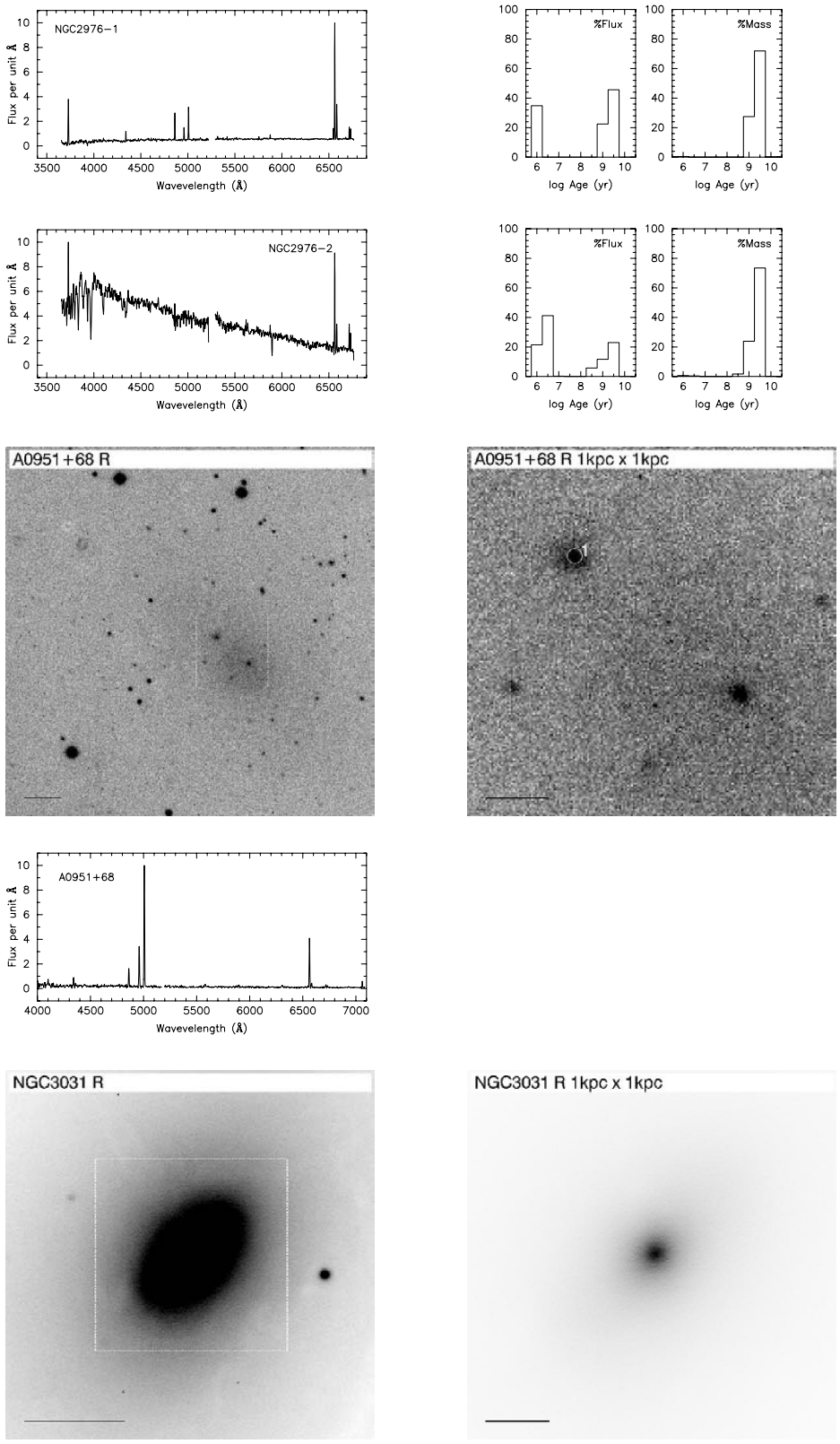

Figure 2 – *continued*

Having said that, a number of studies have shown that even if metallicity estimates for individual galaxies are not reliable, results for samples do reveal systematic and astrophysically meaningful trends. For instance, Cid Fernandes et al. (2005) and Gallazzi et al. (2005) have shown that the mean metallicity correlates with galaxy mass, luminosity and (in the case of star-forming galaxies) gas-phase metallicities. Table 9 shows that metallicity indeed increases with luminosity, as expected from the mass–metallicity relation. There

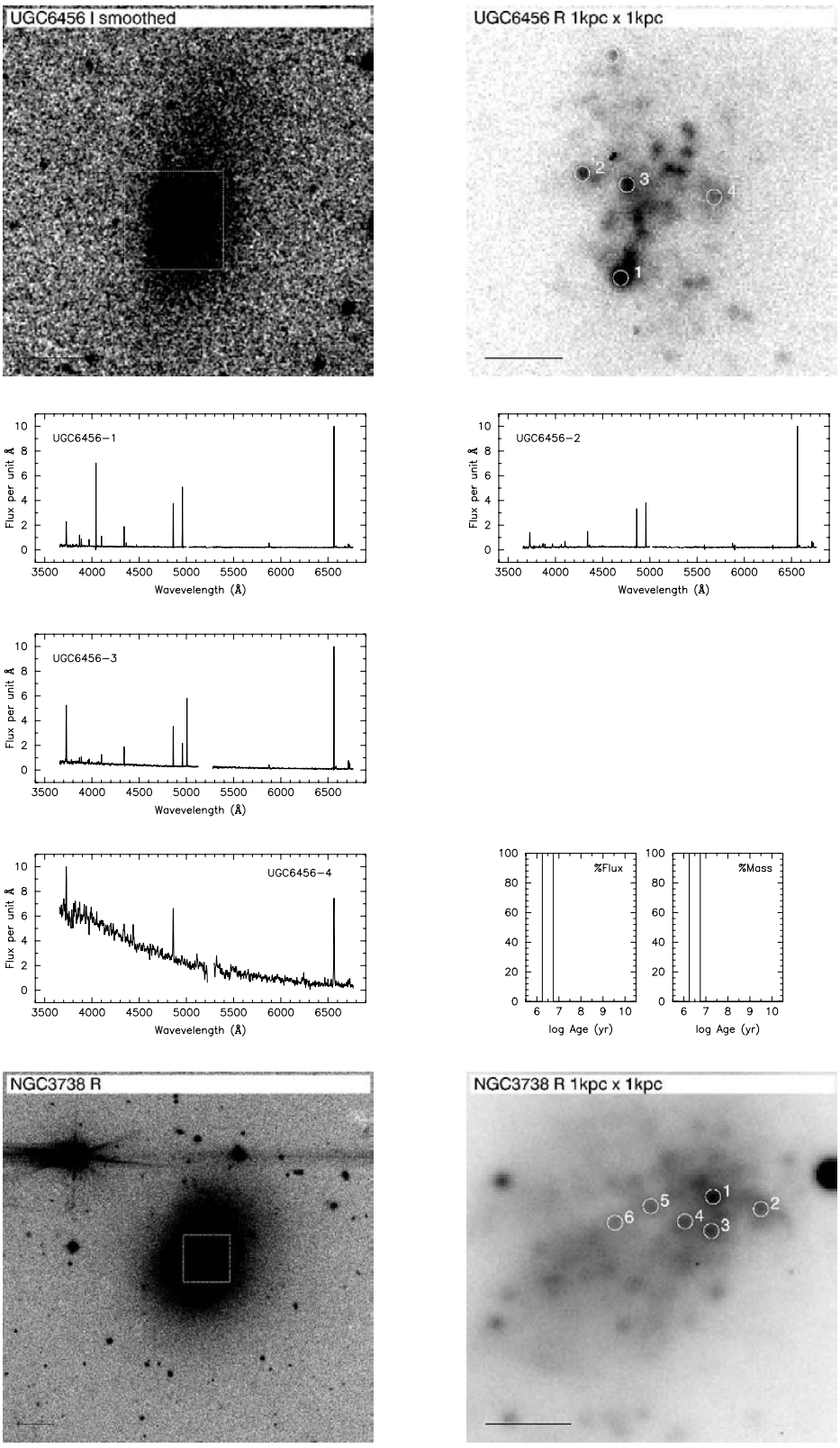

Figure 2 – *continued*

also seems to be a tendency for off-nuclear sources to be more metal poor than galaxy nuclei.

Note that all of the galaxies in the E–S0 Hubble class within our sample are dwarfs such as NGC 185, NGC 205, NGC 404 and NGC 4150, instead of massive ellipticals. As can be seen in Table 9, this class harbours stellar populations with ages distinctively younger and metallicities distinctively lower than early-type spirals.

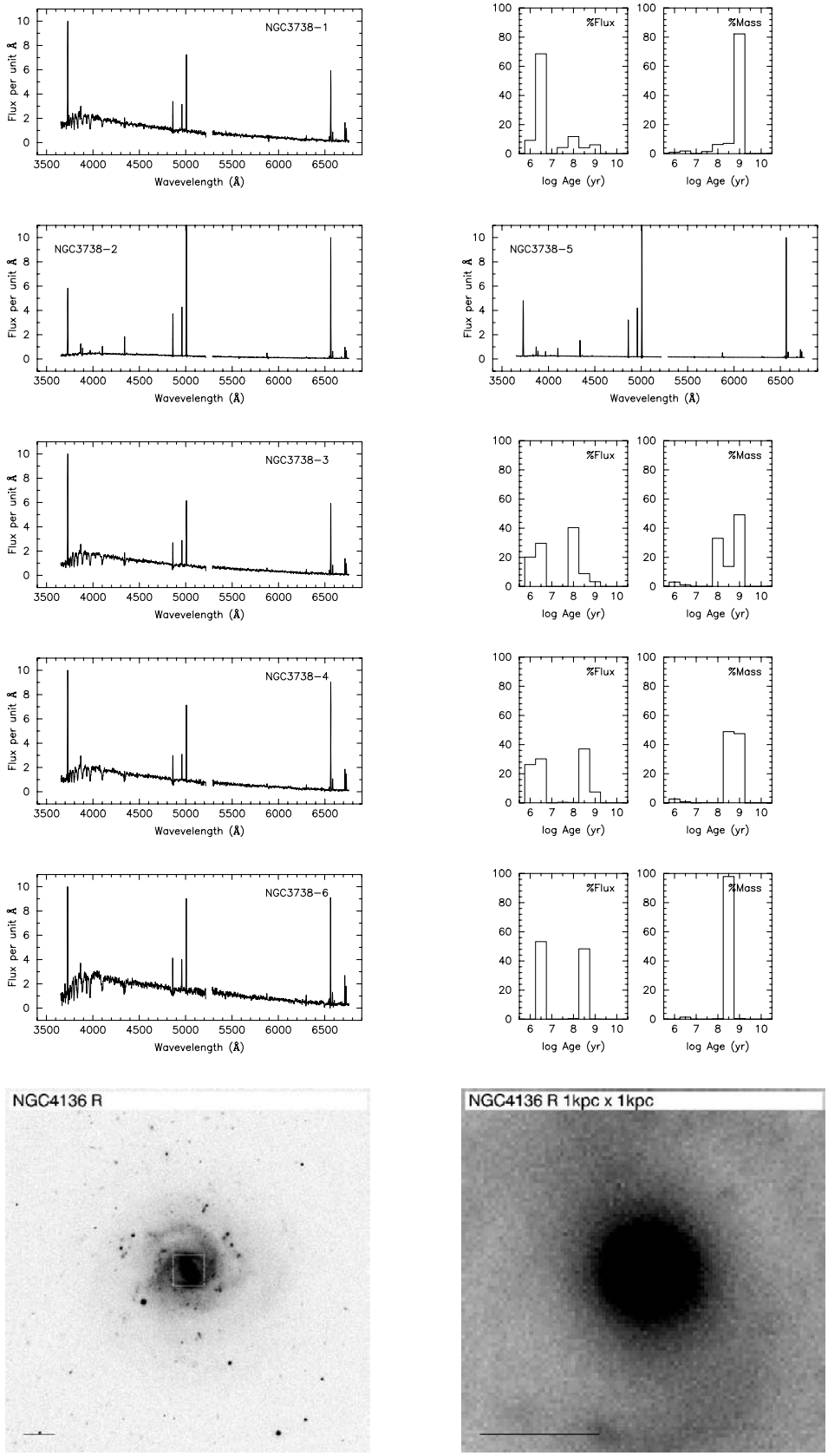

Figure 2 – *continued*

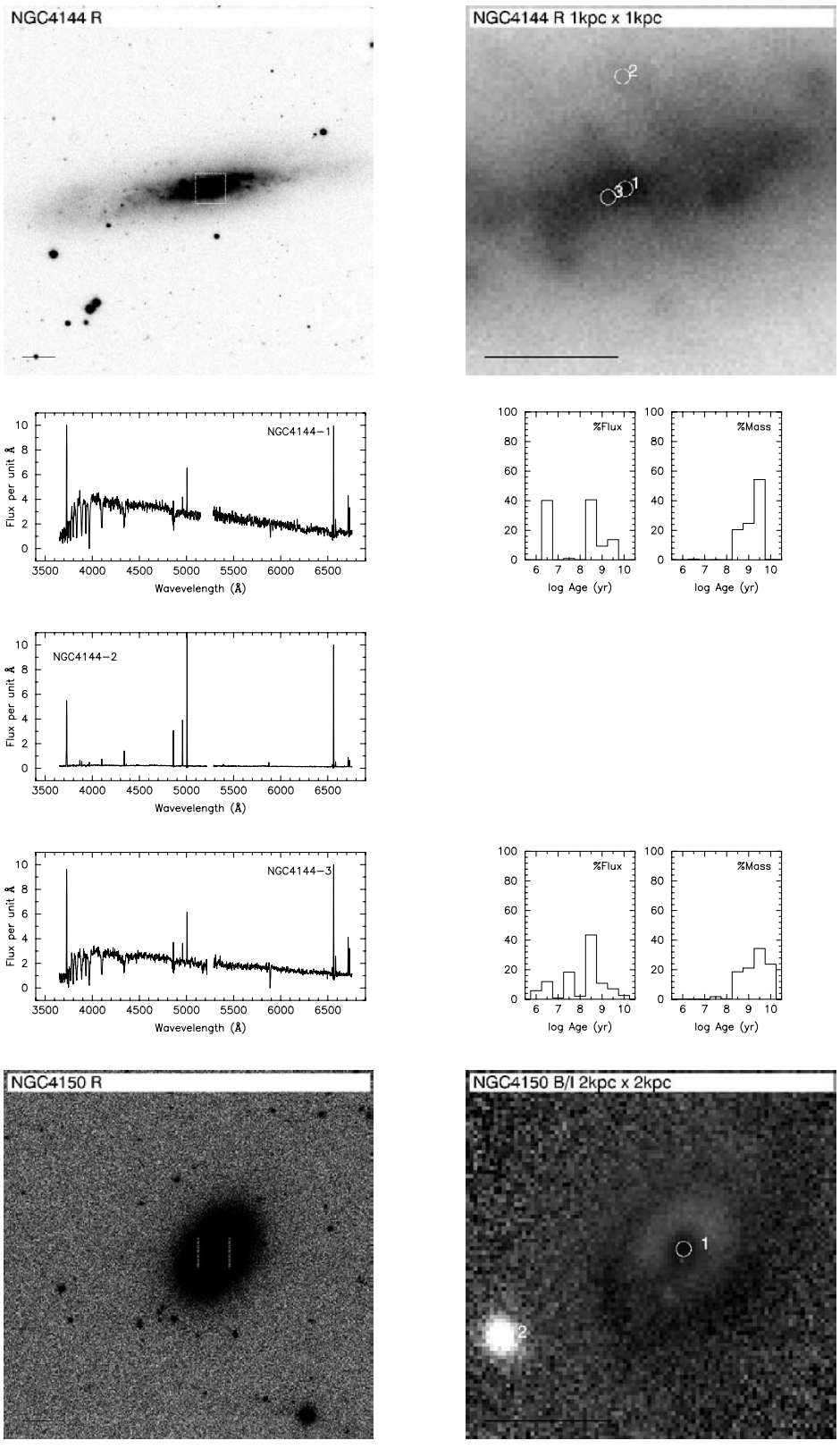

Figure 2 – *continued*

5.2 Gas-phase abundances

Abundances of star-forming regions were estimated using the 'strong line' method as detailed by Pilyugin (2000). For those objects where the very weak, temperature-sensitive [O III] λ4363 line could be measured, a more accurate estimate of the oxygen abundance was also derived (e.g. Pagel et al. 1992). The range in abundances shown in Table 10 spans from $Z/Z_{\odot} \lesssim 0.1$ (NGC 2366,

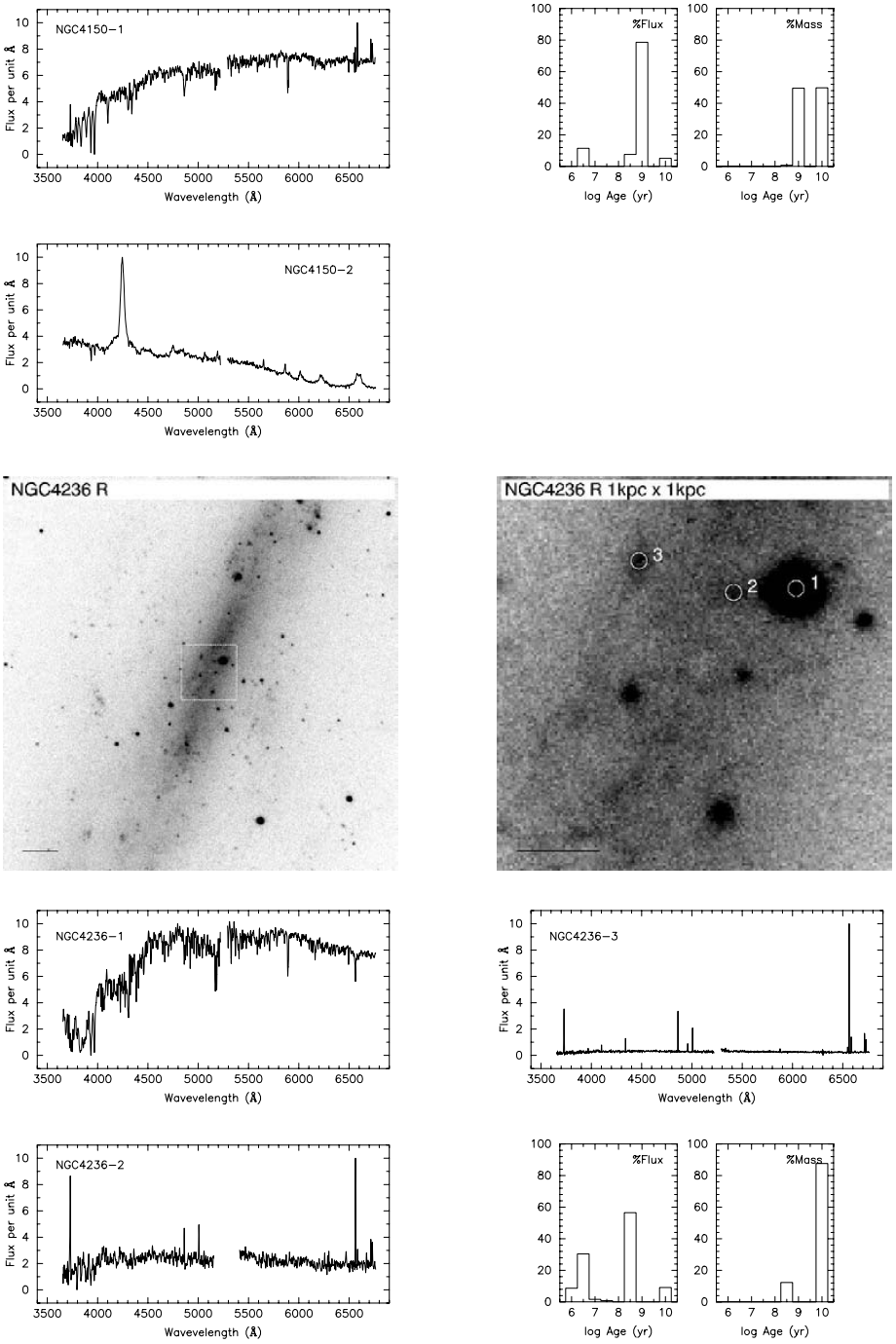

Figure 2 – *continued*

UGC 6456) to solar-rich objects with $Z/Z_{\odot} \gtrsim 1$ (NGC 4236, NGC 4826).

High metallicities determined from nebular measurements are quite uncertain. This is because the [O III] λ4363 line is too weak in metal-rich systems to be detected and, therefore, an accurate calibration of the 'strong line' method has not been determined for such systems (Pilyugin 2000). When both methods have been applied, there is an excellent correspondence between the determined abundances. This is because these sources correspond to pure HIIR spectra with low metallicities and which are not subject to uncertainties due to poorly determined line fluxes.

As discussed in the next section, there is evidence that some of the emission-line spectra might be shock-excited and not only photoionized. In these cases the metallicities derived here would be incorrect.

6 SPECTRAL CLASSIFICATION FROM EMISSION-LINE PROPERTIES

6.1 Star-forming, AGN and LINER nuclei

A successful method to distinguish between different ionizing mechanisms of the galactic ISM uses emission-line ratios that are

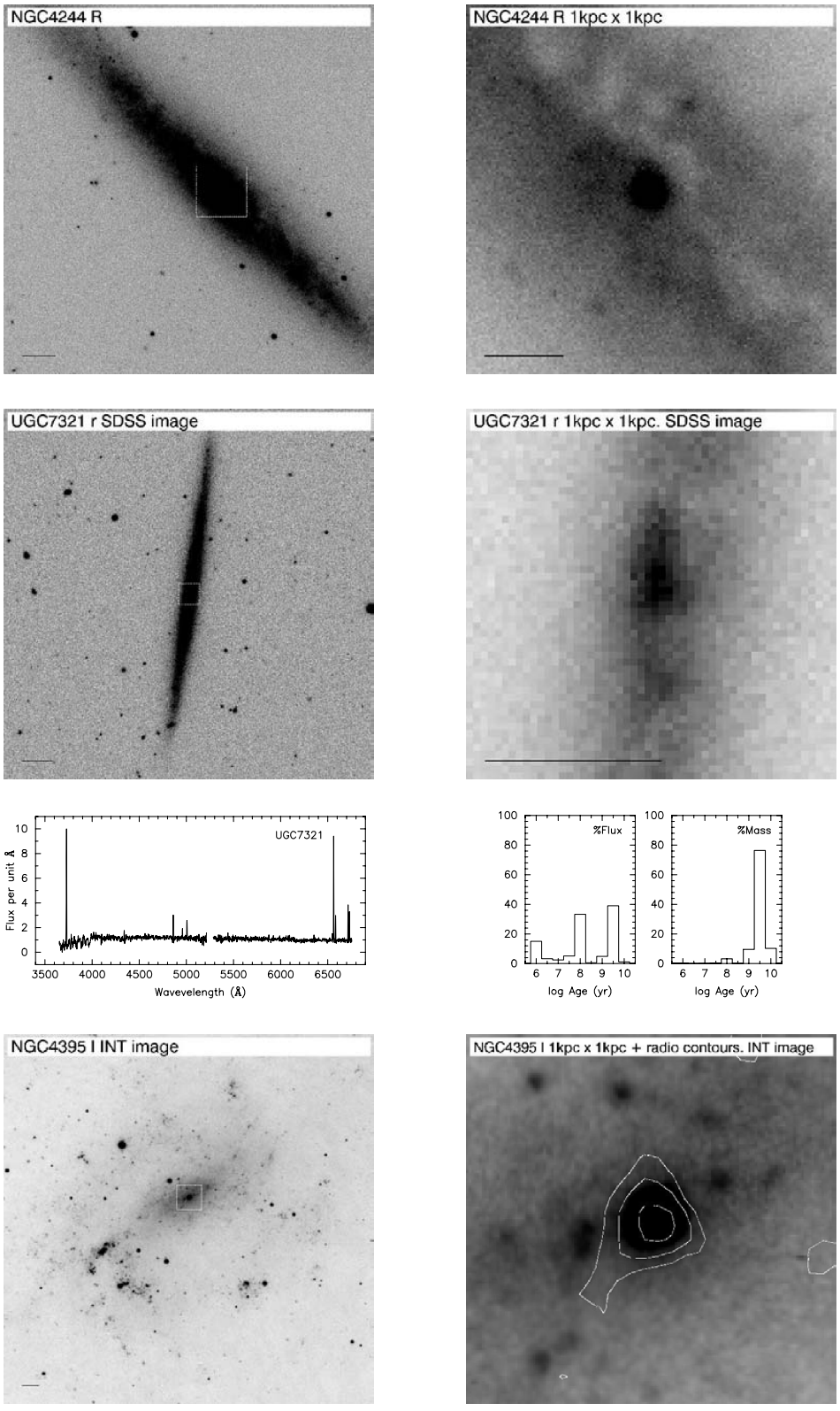

Figure 2 – *continued*

sensitive to changes in the spectral shape of the ionizing radiation (Baldwin, Phillips & Terlevich 1981; Veilleux & Osterbrock 1987; Kewley et al. 2001). In this way diagnostic diagrams can separate the (narrow) nebular emission into three major groups: star-forming regions, AGN and low-ionization nuclear emission-line regions (LINERs).

Theoretical models show that photoionization by hot stars and a non-thermal power-law hard continuum can, respectively,

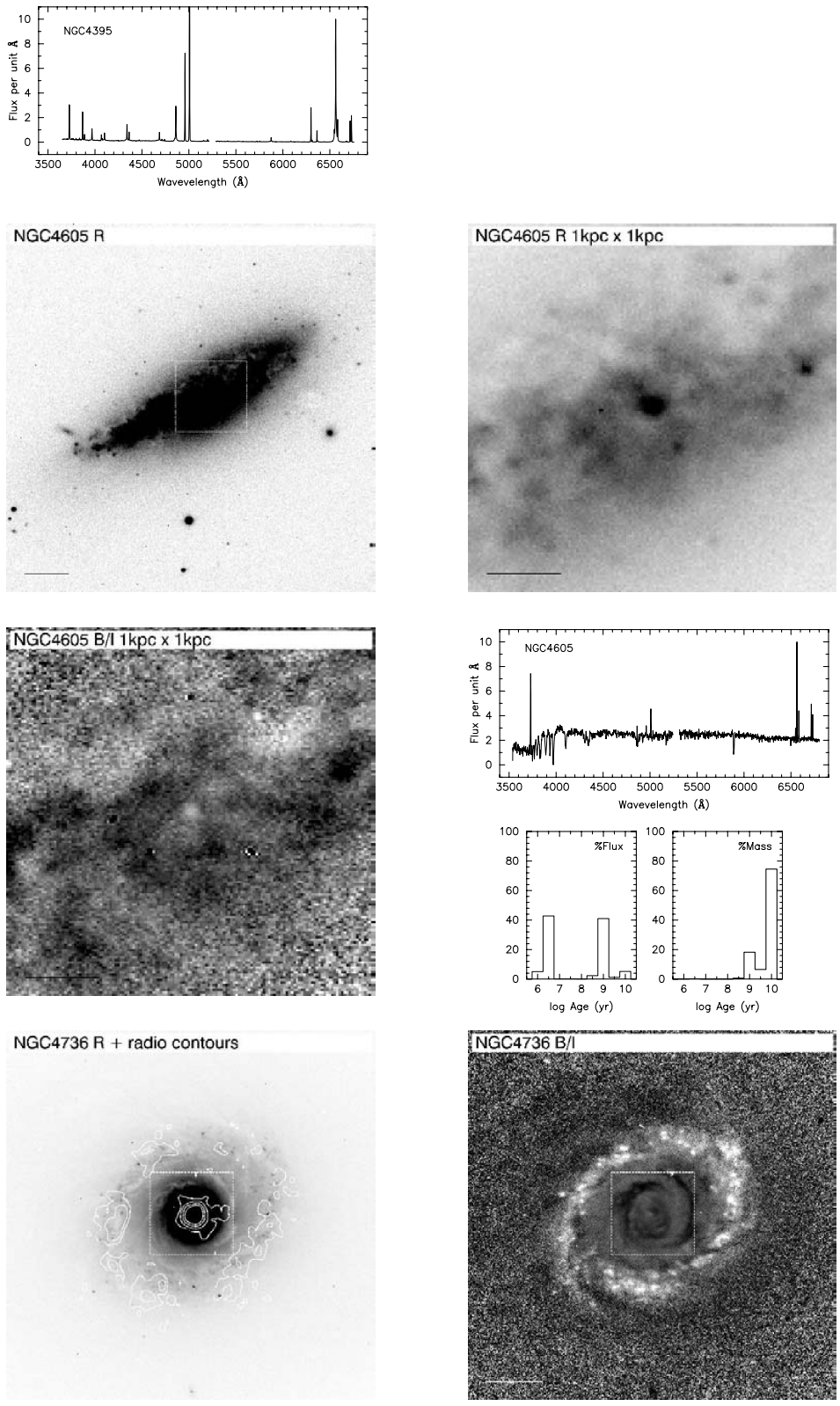

Figure 2 – *continued*

reproduce the line ratios that correspond to the loci occupied in these diagrams by star-forming regions and AGN (see e.g. Veilleux & Osterbrock 1987; Kewley et al. 2001). Fast shocks moving in dense, star-forming-like gas (a 'photoionized precursor') have also been invoked to explain AGN spectra (Dopita & Sutherland 1995), although diagnostics from high-resolution X-ray spectroscopy have recently shown that Seyfert galaxies are indeed photoionized by a hard continuum and not shock-excited (Kaspi et al.

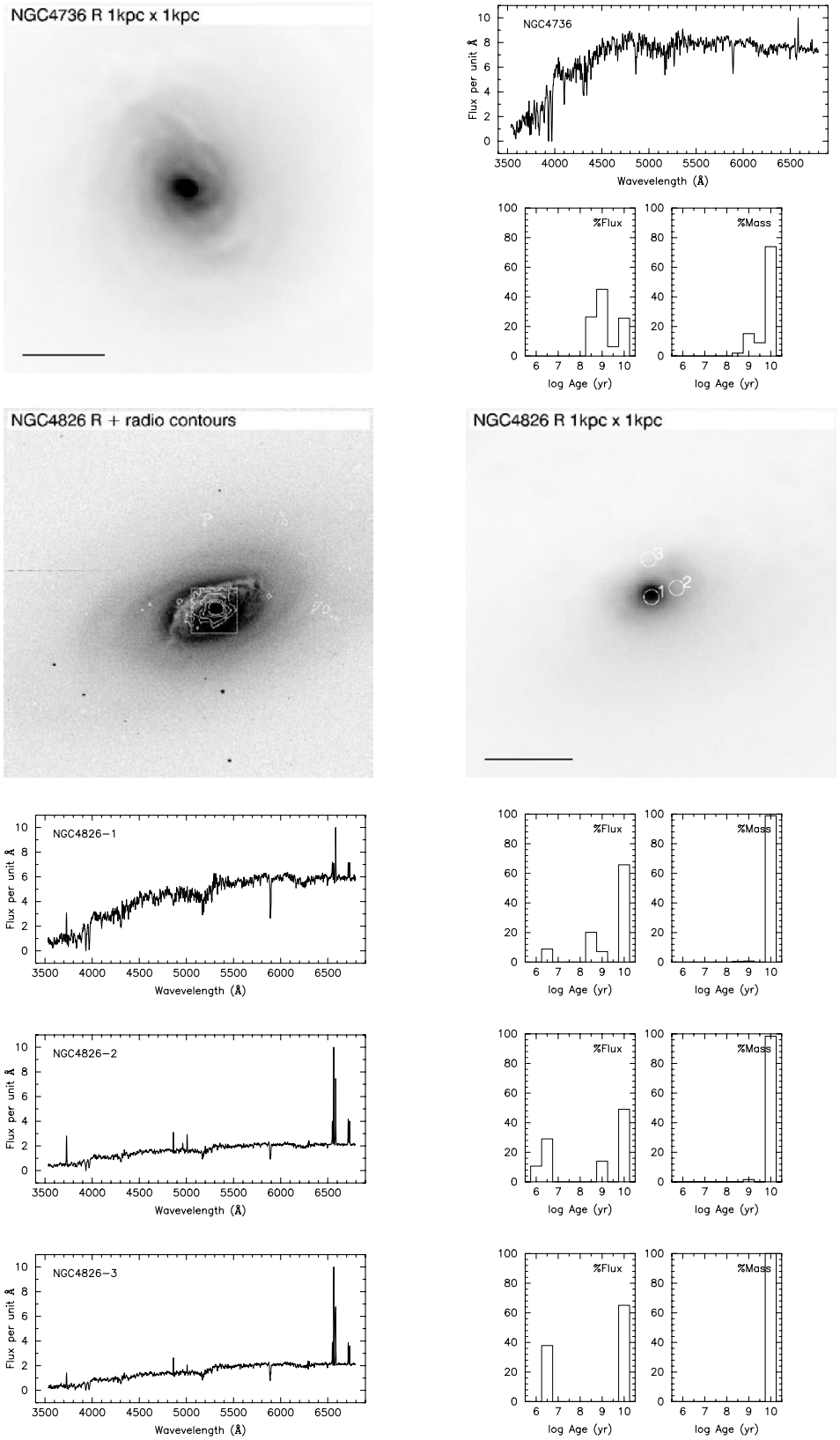

Figure 2 – *continued*

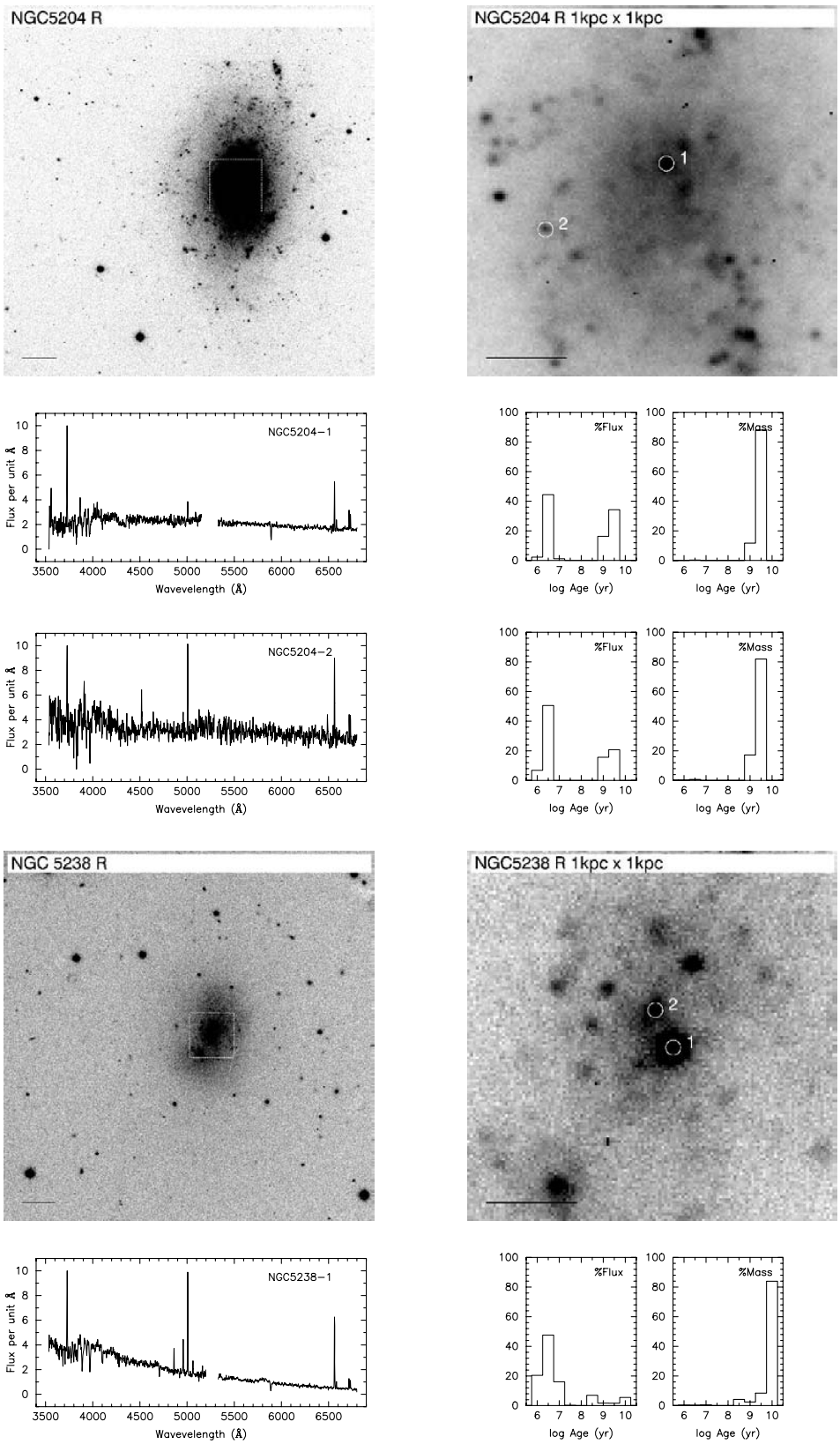

Figure 2 – *continued*

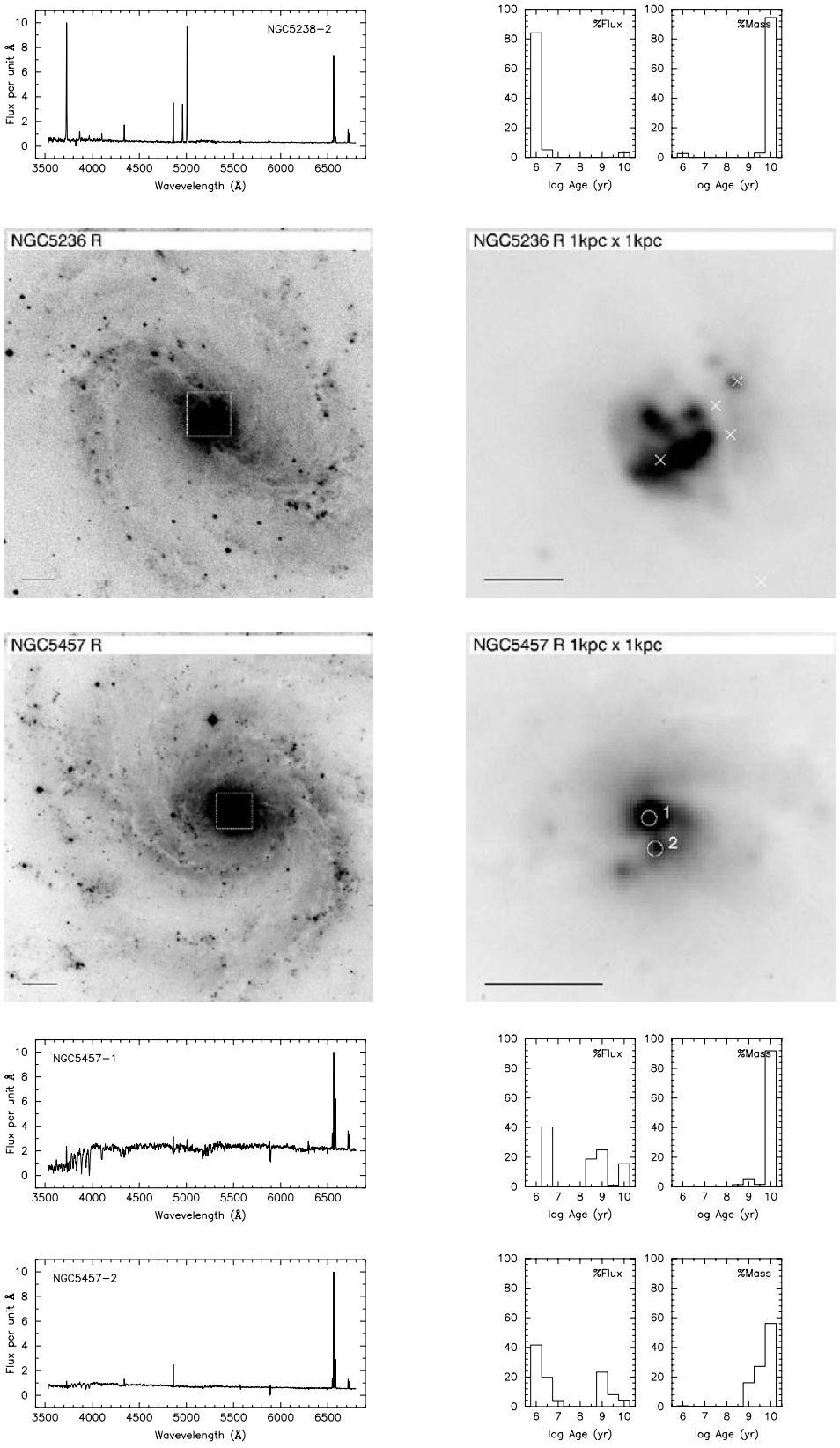

Figure 2 – *continued*

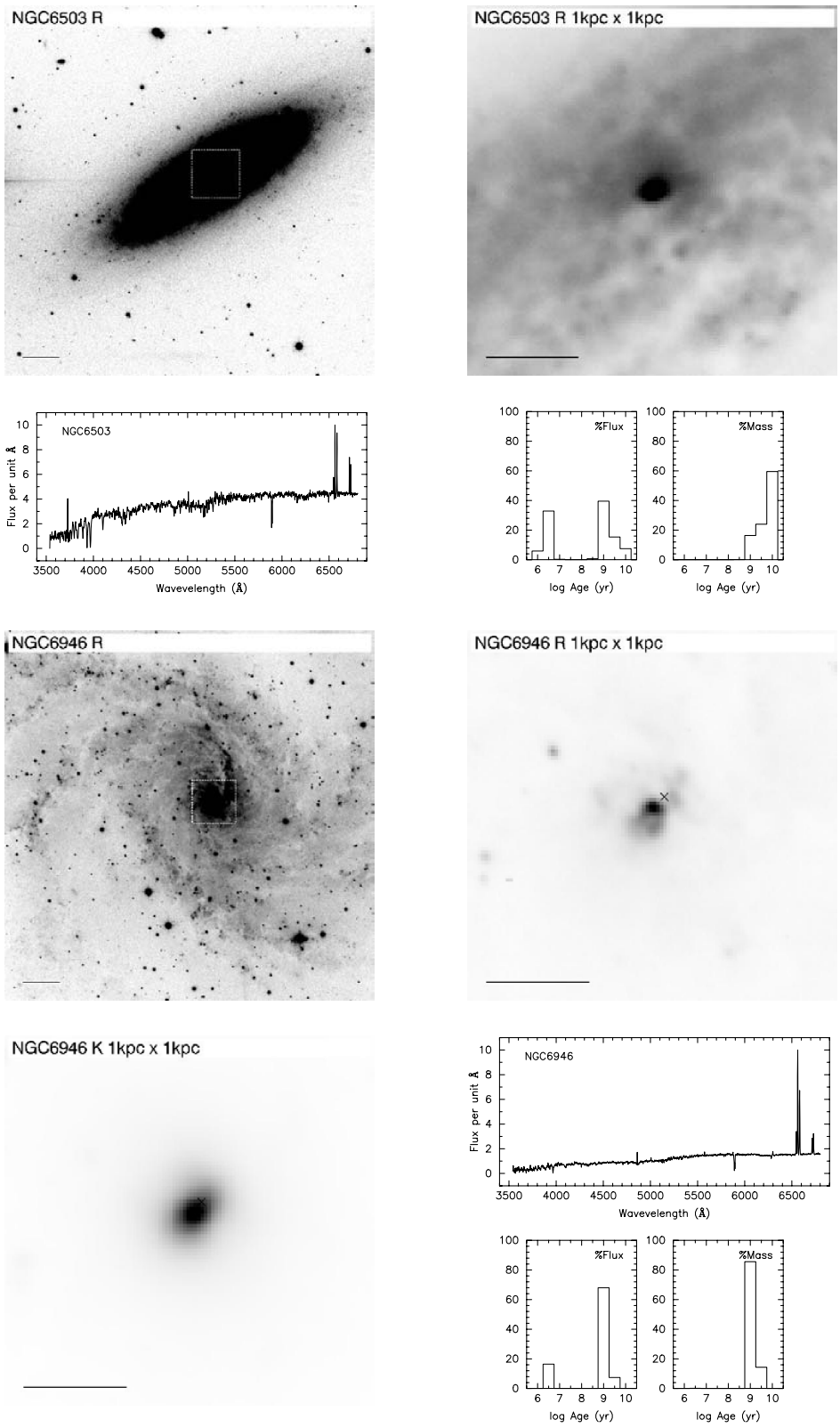

Figure 2 – *continued*

2000 Sako et al. 2000; Sambruna et al. 2001; Brinkman et al. 2002; McKernan et al. 2003; Ogle et al. 2003; Yaqoob et al. 2003).

Heckman (1980) described the LINER class as objects showing oxygen-line ratios so that [O II] λ3727/[O III] λ5007 $\geqslant$ 1.0 and [O I] λ6300/[O III] λ5007 $\geqslant 1/3$. After the introduction of this class many works have used different criteria to classify objects as LINERs (Keel 1983; Ho, Filippenko & Sargent 1995; Kewley et al. 2001). Although not all objects categorized in these ways would

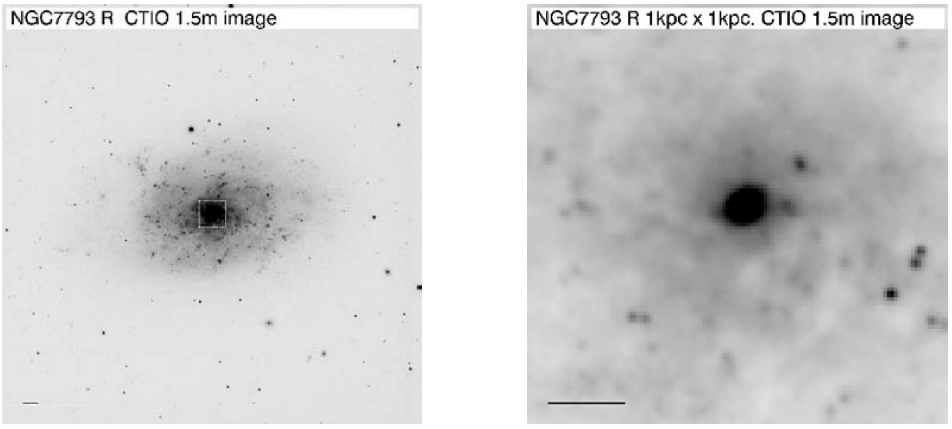

Figure 2 – *continued*

Table 4. Source of images for galaxies without JKT data.

Name	Telescope	Filter
NGC 224	POSS II	Red
NGC 253	LCO 2.5 m	*V*
NGC 598	KPNO 0.9 m	*R*
NGC 1560	POSS II	Red
UGC 7321	SDSS	*r*
NGC 4395	INT	*I*
NGC 7793	CTIO 1.5 m	*R*

comply with the criteria defined by Heckman, they consistently isolate emission-line spectra dominated by low-ionization emission lines. The strength of the (weak) [O I] λ6300 line seems to be the most useful line to classify objects as LINERs.

The nature of LINERs has proven to be a difficult issue to clarify and they most likely correspond to a mixed population of objects. Shock excitation as well as photoionization by AGN or hot stellar continua have been shown to reproduce LINER line ratios (Veilleux & Osterbrock 1987; Dopita et al. 1997; Kim, Veilleux & Sanders 1998; Taniguchi et al. 1999; Alonso-Herrero et al. 2000). Clearly, it is not possible yet to discern between the AGN and the star-forming LINER types solely based on their optical spectra. One of the strongest arguments in support of the classification of at least some LINERs as genuine AGN is that they also show the 'Type 1'/'Type 2' dichotomy (Ho, Filippenko & Sargent 1997b; Barth et al. 2001; Eracleous & Halpern 2001). However, it is also clear that the spectra of many objects that fall into the technical definition of a LINER could, in fact, be of stellar origin (Maoz et al. 1998; Terashima et al. 2000).

Recently, high-resolution X-ray observations have found that 50–60 per cent of LINERs have a dominant, hard point-like source associated with their nuclei (Flohic et al. 2006; Gonzalez-Martin et al. 2006; Satyapal et al. 2006). Although it is likely that some fraction of these sources might correspond to X-ray binaries located in the nuclear region of their host galaxies, this result gives a robust estimate of the fraction of genuine AGN in LINERs. The samples, however, are clearly biased towards luminous galaxies. In fact, of the sample of 82 LINERs studied by Satyapal et al. (2006) less than 3 per cent correspond to galaxies with a *B* absolute magnitude below −17.

6.2 Diagnostic diagrams

Four different diagnostic diagrams were produced using our sample of nearby galaxies. The line fluxes are those presented in Table 6. Note that many galaxies have multiple observations and therefore several data points can belong to the same galaxy. Three of the diagnostic diagrams were originally proposed by Veilleux & Osterbrock (1987) (VO diagrams) and have the advantage of being insensitive to reddening (panels a, b and c in Fig. 3). The fourth diagram, (d), comes from Baldwin et al. (1981) and shows the definition of the LINER class using Heckman's prescription.

In the VO diagrams, we have incorporated the theoretical division between the star-forming, AGN and LINER classes as parametrized by Kewley et al. (2001). The different regions correspond to emission-line ratios produced through photoionization by OB stars in star-forming regions, photoionization by a power-law continuum with a high-ionization parameter or radiative shocks with photoionized precursors in AGN, and photoionization by a power-law continuum with a very low ionization parameter or radiative shocks without photoionized precursors in LINERs. It is important to note that a contribution of as little as ∼20 per cent from an AGN moves the line ratios outside the star-forming region towards the top of the diagrams, showing that this classification is very robust in picking up AGN activity (see Kewley et al. 2001 for details). We have also overlaid MAPPINGS III models showing ionization tracks by fast shocks in an ISM with solar metallicities (Allen et al. 2004).

From the diagnostic diagrams, it can be seen that most data points can be explained as photoionization by hot stars and they are classified as star-forming regions. Panels (b), (c) and (d) also suggest that a handful of our spectra are LINERs. The shock parameters that best fit these data are those with magnetic parameter *b* between 1 and 5 (i.e. in agreement with the 3.2 equipartition value) and for velocities of the order of a few hundred km s^{-1}. In the next section, we will consider the possible nature of these sources. Based on these diagrams we have given a classification to our spectroscopic sources which can be found in Table 5.

Fig. 3 shows two outlying points. They correspond to NGC 4395 and A 0951+68. NGC 4395 has a well-studied dwarf Seyfert nucleus and A 0951+68 is an extreme star-forming region (Johnson, Lawrence & Terlevich 1997) with one of the highest [O III] λ5007/Hβ λ4861 ratios ever observed, hence its unusual location in panels (a), and (b).

Table 5. Coordinates and classification for the sources. When the source corresponds to the galaxy nucleus, this is noted in the last column. Astrometric solutions for our JKT frames were obtained using stars common to our images and either, the APM Catalogue or DSS images. When no JKT images were available, NED coordinates are given. The source classification corresponds to foreground star (FS), stellar (A) (i.e. with total absence of emission lines), star forming (SF), LINER (L) and Seyfert (Sy). An A-SF classification corresponds to a stellar spectrum with very faint superimposed emission lines. For details on the spectral classification, see Section 6.2.

Galaxy-Target	RA (J2000)			Dec. (J2000)			Class	Galaxy-Target	RA (J2000)			Dec. (J2000)			Class
NGC 147-1	0	33	10.55	48	30	34.0	FS	UGC 6456-4	11	27	57.46	78	59	38.6	SF region
NGC 147-2	0	33	11.67	48	30	21.5	FS	NGC 3738-1	11	35	47.44	54	31	32.1	SF region
NGC 185-1	0	38	57.92	48	20	14.7	L region	NGC 3738-2	11	35	46.85	54	31	31.3	SF region
NGC 185-2	0	38	57.59	48	20	12.6	SF region	NGC 3738-3	11	35	47.44	54	31	28.9	SF region
NGC 185-3	0	38	57.31	48	20	15.6	SF region	NGC 3738-4	11	35	47.84	54	31	29.0	SF region
NGC 185-4	0	38	57.76	48	20	19.1	A-SF region	NGC 3738-5	11	35	48.25	54	31	30.7	SF region
NGC 205	0	40	22.00	41	41	07.0	A nucleus	NGC 3738-6	11	35	48.69	54	31	28.7	SF region
NGC 221	0	42	41.76	40	51	54.7	A nucleus	NGC 4136	12	09	17.68	29	55	39.3	SF nucleus[b]
NGC 224	0	42	44.3	41	16	0[a]	A nucleus	NGC 4144-1	12	09	58.37	46	27	26.6	SF region
NGC 247	0	47	08.42	−20	45	42.7	SF nucleus	NGC 4144-2	12	09	58.38	46	27	34.1	SF region
NGC 253	0	47	33.1	−25	17	18[a]	SF nucleus[b]	NGC 4144-3	12	09	58.44	46	27	26.5	SF region
NGC 404	1	09	26.94	35	43	05.3	L nucleus	NGC 4150-1	12	10	33.64	30	24	05.6	L nucleus
NGC 598	1	33	50.9	30	39	36[a]	A-SF nucleus	NGC 4150-2	12	10	34.68	30	23	58.3	Back QSO
MAFFEI 1	2	36	35.52	59	39	17.9	SF nucleus	NGC 4236-1	12	16	42.04	69	27	46.1	FS
MAFFEI 2-1	2	41	54.74	59	36	12.6	SF region	NGC 4236-2	12	16	43.42	69	27	45.2	SF region
MAFFEI 2-2	2	41	55.08	59	36	16.0	SF region	NGC 4236-3	12	16	45.56	69	27	48.5	SF region
MAFFEI 2-3	2	41	55.12	59	36	17.8	SF region	UGC 7321	12	17	34.0	22	32	23[a]	SF region
IC 342-1	3	46	48.50	68	05	47.0	SF nucleus	NGC 4395	12	25	48.9	33	32	48[a]	Sy nucleus
IC 342-2	3	46	48.41	68	05	45.5	SF region	NGC 4605	12	39	59.32	61	36	32.6	SF nucleus
NGC 1560	4	32	49.1	71	52	59[a]	SF region	NGC 4736	12	50	53.04	41	07	14.7	A-SF nucleus
NGC 2366-1	7	28	55.29	69	13	05.4	A cluster	NGC 4826-1	12	56	43.65	21	40	59.0	SF nucleus
NGC 2366-2	7	28	50.14	69	12	21.8	FS	NGC 4826-2	12	56	43.91	21	40	58.0	SF region
NGC 2366-3	7	28	42.40	69	11	22.1	SF region	NGC 4826-3	12	56	43.63	21	41	02.9	SF region
NGC 2366-4	7	28	43.33	69	11	22.7	SF region	NGC 5204-1	13	29	36.50	58	25	12.5	SF nucleus?
NGC 2366-5	7	28	45.62	69	11	26.2	A-SF region	NGC 5204-2	13	31	30.51	58	09	40.4	SF region
NGC 2403-1	7	36	49.97	65	36	03.1	A-SF nucleus	NGC 5238-1	13	34	42.47	51	36	48.6	SF nucleus?
NGC 2403-2	7	36	51.24	65	36	08.9	SF region	NGC 5238-2	13	34	42.70	51	36	52.4	SF region
NGC 2976-1	9	47	15.17	67	55	00.1	SF region	NGC 5236	13	37	00.9	−29	51	57[a]	SF nucleus[b]
NGC 2976-2	9	47	14.27	67	54	55.2	SF region	NGC 5457-1	14	03	12.46	54	20	57.1	SF nucleus
A 0951+68	9	57	07.53	68	35	54.4	SF region	NGC 5457-2	14	03	12.41	54	20	54.6	SF region
NGC 3031	9	55	33.2	69	03	55[a]	Sy nucleus[b]	NGC 6503	17	49	26.38	70	08	39.6	L nucleus
UGC 6456-1	11	28	01.21	78	59	27.9	SF region	NGC 6946	20	34	52.38	60	09	13.4	SF nucleus
UGC 6456-2	11	28	03.13	78	59	40.3	SF region	NGC 7793	23	57	49.8	−32	35	28[a]	SF nucleus[b]
UGC 6456-3	11	28	01.17	78	59	39.4	SF region								

[a]NED Coordinates. [b]Classification adopted from the literature (see Appendix A).

6.3 LINERs in the sample

The diagnostic diagrams presented in Fig. 3 clearly show that no other classical AGN (i.e. characterized by a high-excitation emission-line spectrum) are present in our sample, except for NGC 4395. NGC 3031, which belongs to our sample but was not observed during the spectroscopic follow-up, is also a classical AGN (Peimbert & Torres-Peimbert 1981a; Ho, Filippenko & Sargent 1996). All other targets are consistent with a classification as star-forming regions or LINERs. However, as already mentioned, there is evidence that not all LINERs are driven by the same physical processes.

We determined which sources fall systematically in the LINER region where shock excitation or photoionization with a low-ionization parameter is expected to be the dominant ionization process. The results are shown in Table 11.

Some caveats have to be taken into account when examining Fig. 3. As can be seen, all data points lie to the left-hand side of the LINER region in panel (a), and the [N II] λ6584/Hα ratios from models of shock excitation also fail to reach the LINER region (see also Allen et al. 2004). This is because the theoretical line defining the border of the starburst loci is determined by the *highest* possible line ratios as predicted by star-forming models, and for [N II] λ6584/Hα there is a clear overlap in the values shown by pure star-forming regions and LINERs, moving the border into LINER territory. Hence, panel (a) does not seem like a good diagnostic to discriminate between these classes of objects. Next, variations in density can introduce uncertainties in the classification drawn from the [S II] λλ6717,6730/Hα (panel b) and an object should not be classified as a LINER based purely on this diagnostic (Kewley et al. 2001). Finally, it should be noted that panel (d) is highly biased against spectra of star-forming regions as the O I line becomes extremely weak in these regions. As can be seen from Table 6 measurements of this line are quite uncertain for many objects.

Based on the results from Table 11 we adopt a LINER classification for NGC 185, NGC 404, NGC 4150, NGC 4736, NGC 4826 and NGC 6503, giving a LINER fraction of ∼18 per cent (6/33) for our sample. These objects do not show any evidence of broad components to their permitted lines, which classifies them as narrow-line ('type 2') LINERs. In what follows we will examine the possible nature of these sources.

Table 6. Line flux ratios with respect to the Hα emission line. The values have been corrected by external and internal extinction.

Galaxy-Target	[O II] λ3727	Hδ λ4102	Hγ λ4340	[O III] λ4363	Hβ λ4861	[O III] λ5007	HeI λ5876	[OI] λ6300	[N II] λ6584	[S II] λ6717	[S II] λ6730
NGC 185-1	2.519	–	–	–	0.549	1.048	–	0.603	0.533	0.790	0.580
NGC 185-2	2.318	–	–	–	0.456	0.739	–	–	0.601	0.700	0.576
NGC 185-3	–	–	–	–	0.364[a]	0.441[a]	–	–	0.360	0.281	0.172
NGC 185-4	–	–	–	–	–	–	–	–	0.642	0.390[a]	0.675[a]
NGC 247	–	–	–	–	0.505	0.576[a]	–	–	0.248	0.281	0.224
NGC 404	1.366	–	0.205	–	0.358	0.452	–	0.229	0.462	0.522	0.428
NGC 598	–	–	–	–	0.653[a]	1.324[a]	–	–	0.859[a]	–	–
IC 342-1	–	0.107[a]	0.221[a]	–	0.357	0.071	0.030	–	0.470	0.100	0.128
IC 342-2	–	0.176	0.191	–	0.357	0.045	0.063	–	0.394	0.076	0.091
NGC 1560	0.773	0.094	0.165	0.024	0.358	1.078	0.040	–	0.052	0.064	0.048
NGC 2403-2	–	–	–	–	0.677	–	–	–	0.624	0.492[a]	0.661[a]
NGC 2366-3	0.123	0.091	0.181	0.066	0.358	2.878	0.039	0.003	0.006	0.009	0.008
NGC 2366-4	0.344	0.103	0.198	0.060	0.425	2.128	0.039	–	0.016	0.025	0.020
NGC 2366-5	0.381	0.096	0.169	0.046	0.383	1.788	0.042	–	0.019	0.035	0.025
NGC 2976-1	0.938	0.125	0.161	–	0.359	0.392	0.045	–	0.300	0.108	0.093
NGC 2976-2	0.756	–	0.279[a]	–	0.358	0.140	0.092	–	0.202	0.214	0.127
A 0951+68	–	0.153	0.181	–	0.357	2.736	–	–	0.094	0.042	0.028
UGC 6456-1	0.297	0.098	0.176	0.037	0.382	1.455	0.040	–	0.016	0.030	0.021
UGC 6456-2	0.201	0.067	0.140	0.025	0.362	1.141	0.041	–	0.020	0.053	0.042
UGC 6456-3	0.677	0.088	0.162	–	0.362	0.594	0.035	–	0.027	0.070	0.050
UGC 6456-4	0.613	–	–	–	0.809	0.153[a]	–	–	–	0.090[a]	0.101[a]
NGC 3738-1	1.631	0.111	0.216	–	0.488	1.042	–	0.053	0.125	0.247	0.186
NGC 3738-2	0.784	0.071	0.158	0.027	0.366	1.242	0.038	0.013	0.063	0.096	0.071
NGC 3738-3	1.940	0.155	0.264	–	0.418	0.884	0.042	0.056	0.139	0.233	0.168
NGC 3738-4	1.450	0.096	0.169	–	0.375	0.787	0.040	0.051	0.121	0.226	0.166
NGC 3738-5	0.889	0.089	0.169	0.018	0.358	1.388	0.038	0.010	0.047	0.068	0.048
NGC 3738-6	1.432	0.166	0.205	–	0.457	0.809	0.067	0.056	0.108	0.267	0.181
NGC 4144-1	1.329	0.166	0.218	–	0.357	0.449	–	–	0.174	0.375	0.240
NGC 4144-2	1.109	0.083	0.156	0.020	0.358	1.306	0.036	–	0.046	0.073	0.054
NGC 4144-3	1.197	0.106	0.192	–	0.368	0.476	–	–	0.179	0.315	0.236
NGC 4150-1	1.522	–	0.307[a]	–	0.359	0.706	–	0.209[a]	0.921	0.658	0.523
NGC 4236-2	1.135	0.319[a]	0.213[a]	–	0.507	0.449	–	–	0.116	0.266	0.266
NGC 4236-3	0.666	0.076	0.127	–	0.358	0.227	0.027	–	0.126	0.159	0.111
UGC 7321	2.052	0.172	0.221	–	0.358	0.278	–	–	0.232	0.359	0.270
NGC 4395	0.629	0.095	0.209	0.120	0.411	3.862	0.059	0.413	0.241	0.273	0.331
NGC 4605	1.326	0.128	0.200	–	0.358	0.373	–	–	0.285	0.322	0.208
NGC 4736	1.586	–	–	–	0.358[a]	0.567[a]	–	0.404[a]	1.603	0.631	0.543
NGC 4826-1	2.603	–	–	–	0.360	0.734	–	0.237[a]	1.575	0.708	0.635
NGC 4826-2	0.651	0.091	0.169	–	0.358	0.326	–	0.088[a]	0.710	0.296	0.257
NGC 4826-3	0.431	0.091	0.149	–	0.359	0.219	–	0.072[a]	0.607	0.241	0.205
NGC 5204-1	2.152	–	0.254	–	0.397	0.368	–	–	0.251	0.353	0.288
NGC 5204-2	1.188	–	–	–	0.413	0.829	–	–	0.163[a]	0.289	0.282
NGC 5238-1	1.416	–	0.296	–	0.536	1.286	–	0.074[a]	0.110	0.150	0.124
NGC 5238-2	1.634	0.108	0.207	–	0.461	1.315	0.061	–	0.083	0.157	0.118
NGC 5457-1	0.406	0.112	0.164	–	0.359	0.194	0.029[a]	0.040[a]	0.503	0.214	0.157
NGC 5457-2	0.116	0.105	0.193	–	0.359	0.024	–	–	0.264	0.081	0.063
NGC 6503	1.187	–	0.202	–	0.358	0.352	–	0.112	0.697	0.468	0.335
NGC 6946	–	–	–	–	0.364	0.152	–	0.044	0.585	0.142	0.159

[a]Uncertain flux measurements.

The dwarf galaxy NGC 185 was classified as a Seyfert 2 by Ho et al. (1997a) based on their spectrum of the source they identified as the nucleus. A comparison of our spectra with the data published by Ho et al. (1997a) suggests that this corresponds to source 2.

It is clear from panel (d) in Fig. 3 that the [O II] λ3727/[O III] λ5007 ratio alone is able to distinguish between Seyfert and LINER nuclei, since Seyferts have [O II] λ3727/[O III] λ5007 $\lesssim 0.6$ while LINERs have [O II] λ3727/[O III] λ5007 $\gtrsim 1.0$. This line ratio was not available to Ho et al. (1997a), but our data for NGC 185 imply [O II] λ3727/[O III] λ5007 $\sim$3.2. Note that a sub-estimation of the extinction correction will make the ratio even larger. In fact, the spectroscopy of three different emission knots in NGC 185 has line ratios consistent with those of SNRs (Galarza, Walterbos & Braun 1999). The total extent of the Hα nebula is $\sim$50 pc, has a total luminosity of 1.3×10^{36} erg s^{-1}, and is displaced towards east from the nucleus of the galaxy by $\sim$20 arcsec (Young & Lo 1997).

As already mentioned, a LINER spectrum can be explained by shock excitation. This mechanism is expected to dominate in young star-forming regions, where SNRs deposit large amounts of mechanical energy into the ISM. The presence of extended radio or X-ray emission would favour this scenario.

Our radio observations of NGC 404 show a marginally resolved nuclear source, while ultraviolet (UV) spectroscopic observations show that this nucleus is dominated by stellar absorption features

Table 7. Foreground and intrinsic extinction values for our spectra. Galactic extinctions in the line of sight were taken from Schlegel et al. (1998). Extinctions towards the nebular components were derived using Balmer decrement measurements while stellar extinctions were obtained from the population-synthesis analysis.

Galaxy	A_V (galactic)	A_V (nebular)	A_V (stellar)	Galaxy	A_V (galactic)	A_V (nebular)	A_V (stellar)
NGC 185-1	0.56	0.00[a]	0.46	NGC 3738-2	0.03	0.00	—
NGC 185-2	0.56	0.00	0.47	NGC 3738-3	0.03	0.00	0.72
NGC 185-3	0.56	3.15[a]	0.53	NGC 3738-4	0.03	0.00	0.59
NGC 185-4	0.56	—	0.63	NGC 3738-5	0.03	0.39	—
NGC 205	0.19	—	0.00	NGC 3738-6	0.03	0.00	0.45
NGC 221	0.19	—	0.00	NGC 4144-1	0.05	0.08	0.46
NGC 224	0.19	—	0.00	NGC 4144-2	0.05	0.48	—
NGC 247	0.06	0.00	0.59	NGC 4144-3	0.05	0.00	0.54
NGC 404	0.18	0.38	0.66	NGC 4150-1	0.06	0.69	0.89
NGC 598	0.13	0.00[a]	0.00	NGC 4236-1	0.05	—	0.00
IC 342-1	1.73	0.61	0.00	NGC 4236-2	0.05	0.00	0.42
IC 342-2	1.73	0.63	0.00	NGC 4236-3	0.05	0.24	—
NGC 1560	0.58	0.30	0.72	UGC 7321	0.09	0.42	0.69
NGC 2366-1	0.11	—	—	NGC 4395	0.05	0.00[b]	—
NGC 2366-2	0.11	—	0.00	NGC 4605	0.04	0.18	1.09
NGC 2366-3	0.11	0.24	—	NGC 4736	0.06	0.40[a]	0.20
NGC 2366-4	0.11	0.00	—	NGC 4826-1	0.13	1.44	0.54
NGC 2366-5	0.11	0.00	—	NGC 4826-2	0.13	0.42	0.72
NGC 2403-1	0.12	—	0.30	NGC 4826-3	0.13	0.73	0.89
NGC 2403-2	0.12	0.00	0.84	NGC 5204-1	0.04	0.00	0.57
NGC 2976-1	0.21	0.89	1.23	NGC 5204-2	0.04	0.00	1.10
NGC 2976-2	0.21	0.06	0.29	NGC 5238-1	0.03	0.00	0.76
A 0951+68	0.22	0.15	—	NGC 5238-2	0.20	0.00	1.80
UGC 6456-1	0.11	0.00	—	NGC 5457-1	0.03	0.72	0.73
UGC 6456-2	0.11	0.00	—	NGC 5457-2	0.03	0.96	0.75
UGC 6456-3	0.11	0.00	—	NGC 6503	0.10	0.59	1.25
UGC 6456-4	0.11	0.00	0.99	NGC 6946	1.06	3.55	1.78
NGC 3738-1	0.03	0.00	0.52				

[a]Uncertain values due to poor line flux determinations (see Table 6). [b]For the Seyfert nuclei in NGC 4395, an intrinsic value of Hα/Hβ = 3.1 was assumed.

from young stars (Maoz et al. 1998). Upper limits are available for NGC 185, NGC 4150 and NGC 6503 at radio wavelengths. As can be seen from Fig. 2, NGC 4736 and NGC 4826 present complex, extended nuclear radio emission. Two of the radio sources in NGC 4826 show SNR-like spectra.

The detection of a point-like X-ray source is one of the best diagnostics for the presence of an AGN. An analysis of *ROSAT* HRI data in Paper I showed the presence of a weak nuclear X-ray source in NGC 404, extended X-ray emission in NGC 4736 and NGC 4826, and gave an upper limit of $L_{2-10\,\mathrm{keV}} < 5 \times 10^{36}$ erg s^{-1} for NGC 185 (assuming a power-law spectral distribution with $\Gamma = 1.5$ and extrapolating from the *ROSAT* 0.1–2.4 keV band to the 2–10 keV energy range).

High-resolution *Chandra* imaging is now available for 5/6 of our LINERs. For NGC 404 *Chandra* shows that the nuclear emission corresponds to a resolved, compact star-forming region (Eracleous et al. 2002). The nuclear region in NGC 4736 presents several point-like sources embedded in complex diffuse emission and Eracleous et al. (2002) and Pellegrini et al. (2002) interpreted these sources as binaries associated with the strong star-forming episode (but see Gonzalez-Martin et al. 2006). *Chandra* also gives an upper limit of $L_{2-10\,\mathrm{keV}} < 10^{38}$ erg s^{-1} for a nuclear source in NGC 4826 (Ho et al. 2001; Dudik et al. 2005; Pellegrini 2005).

Finally, *Chandra* observations for NGC 4150 and NGC 6503 are presented in Appendix B. Although the X-ray flux for a nuclear source in NGC 6503 has already been presented by Satyapal et al. (2006), the nucleus was misidentified in that work. The analysis presented in the appendix shows that the emission in NGC 4150 and NGC 6503 is dominated by point sources, with only a weak source ($L_{2-10\,\mathrm{keV}} = 2 \times 10^{37}$ erg s^{-1}) being coincident with the galactic nucleus in NGC 6503. For NGC 4150 only an upper limit ($L_{2-10\,\mathrm{keV}} < 4 \times 10^{38}$ erg s^{-1}) is found.

Thus, none of our LINERs is a strong AGN candidate, lacking the presence of a *dominant* hard point-like source associated with their nuclei. The only galaxy without *Chandra* data, NGC 185, also has a tight upper limit for a hard X-ray source from the *ROSAT* observations, unless the source has some degree of obscuration. Ho et al. (2001) determined a $L_{2-8\,\mathrm{keV}}$–$L_{\mathrm{H}\alpha}$ correlation for type 1 AGN ranging from low-z quasi-stellar objects (QSOs) to type 1 LINERs. The somewhat large scatter in the correlation (given the small range in luminosities we are probing), however, allows for all our objects (adopting the Hα fluxes measured by Ho et al. 1997a) to be still consistent with the presence of an AGN. Therefore, it is not possible to *prove* that there is no AGN activity in the nuclei of these sources, but given the clear presence of star-forming activity that can account for the observed nebular emission in the nuclear regions of NGC 185, NGC 404, NGC 4736 and NGC 4826, we find that the evidence for AGN activity is very weak.

To summarize, there is no *unambiguous* AGN-related LINER in our sample. Still, given their X-ray properties, NGC 4150 and NGC 6503 remain possible candidates for AGN activity in LINERs. Clearly, the presence of an AGN has not been completely ruled out in the other LINER nuclei, but AGN activity does not seem to be the *main* mechanism responsible for the observed nuclear properties.

Table 8. Results from the spectral synthesis technique for our targets. Stellar velocity dispersions with values less than 50 km s^{-1} are set to $\sigma_\star < 50$ km s^{-1}. Percentage fluxes at 4020 Å and masses are given for three age groups [a young component ($t < 10^8$ yr), an intermediate component ($10^8 < t < 1.4 \times 10^9$ yr) and an old component ($t > 10^9$ yr)].

Galaxy	Hubble type	$\sigma_\star$ (km s^{-1})	Flux (Y) (per cent)	Flux (I) (per cent)	Flux (O) (per cent)	Mass (Y) (per cent)	Mass (I) (per cent)	Mass (O) (per cent)
NGC 185-1	dE3	63	47.0	37.2	15.8	0.3	15.0	84.7
NGC 185-2	”	<50	51.9	38.1	10.0	0.4	12.1	87.5
NGC 185-3	”	77	48.5	22.5	29.0	0.5	36.2	63.3
NGC 185-4	”	<50	58.4	27.2	14.4	0.5	15.9	83.6
NGC 205	S0/E5	<50	0.0	87.9	12.1	0.0	69.6	30.3
NGC 221	E2	57	0.0	10.4	89.6	0.0	2.1	97.8
NGC 224	Sb	186	0.0	1.1	98.9	0.0	0.1	100.0
NGC 247	Sc(s)	<50	50.7	44.3	4.9	2.0	53.5	44.6
NGC 404	S0	<50	19.5	68.0	12.5	0.1	24.2	75.7
NGC 598	Sc(s)	<50	0.0	100.0	0.0	0.0	99.9	0.1
MAFFEI 1	E3	141	69.0	0.0	31.0	1.1	0.0	98.9
IC 342-1	S(B)cd(rs)	<50	77.1	22.9	0.0	27.4	72.2	0.4
IC 342-2	”	<50	100.0	0.0	0.0	99.8	0.1	0.1
NGC 1560	Sd(s)	210	97.0	0.0	3.0	4.2	0.0	95.8
NGC 2366-1	SBm	90	73.3	0.0	26.7	0.3	0.0	99.7
NGC 2366-2	”	80	0.0	26.4	73.6	0.0	6.0	94.0
NGC 2403-1	Sc(s)	122	7.3	29.7	63.0	0.0	13.1	87.0
NGC 2403-2	”	75	10.1	53.0	36.9	0.1	13.4	86.5
NGC 2976-1	Sd	136	33.8	9.8	56.4	0.9	11.3	87.8
NGC 2976-2	”	172	60.9	16.8	22.3	1.7	27.4	71.0
UGC 6456-4	Peculiar	451	100.0	0.0	0.0	100.0	0.0	0.0
NGC 3738-1	Sd	163	78.8	17.0	4.2	6.5	29.6	63.9
NGC 3738-3	”	<50	48.7	50.1	1.2	6.1	70.7	23.2
NGC 3738-4	”	<50	56.0	41.2	2.9	5.4	64.4	30.2
NGC 3738-6	”	116	52.1	47.9	0.0	2.3	97.8	0.0
NGC 4144-1	Scd	57	39.3	47.3	13.4	0.8	47.0	52.1
NGC 4144-3	”	<50	36.0	53.1	10.9	2.9	39.2	57.7
NGC 4150-1	S0/a	93	11.2	83.7	5.1	0.0	54.8	45.2
NGC 4236-1	SBd	<50	0.0	0.0	100.0	0.0	0.0	100.0
NGC 4236-2	”	123	38.8	52.7	8.5	0.2	14.8	84.9
UGC 7321	Scd	<50	24.7	32.7	42.7	0.9	4.4	94.8
NGC 4605	Sc(s)	<50	49.1	43.7	7.2	0.4	20.3	79.3
NGC 4736	RSab(s)	91	0.0	44.5	55.5	0.0	6.1	93.9
NGC 4826-1	Sab(s)	70	8.8	26.6	64.6	0.0	1.4	98.7
NGC 4826-2	”	88	38.6	13.5	47.9	0.1	1.8	98.1
NGC 4826-3	”	100	36.8	0.0	63.2	0.0	0.0	100.0
NGC 5204-1	Sd	109	48.6	16.3	35.1	0.6	12.4	87.0
NGC 5204-2	”	<50	61.2	16.7	22.1	1.5	18.5	80.0
NGC 5238-1	S(B)dm	185	84.2	7.3	8.5	2.0	5.3	92.6
NGC 5238-2	”	<50	96.5	0.0	3.5	5.1	0.0	94.9
NGC 5457-1	Sc(s)	<50	40.3	42.7	17.0	0.1	7.5	92.4
NGC 5457-2	”	<50	64.7	20.5	14.7	1.2	12.9	85.9
NGC 6503	Sc(s)	<50	38.3	34.3	27.5	0.2	16.5	83.2
NGC 6946	Sc(s)	217	17.8	74.1	8.1	0.1	86.8	13.1

Table 12 gives the final classification adopted for the galaxies in our sample.

7 THE ACTIVE GALACTIC NUCLEUS POPULATION

7.1 AGN fraction and Eddington ratios

These days it is widely assumed that all *massive* galaxies harbour massive black holes in their nuclei. The level of activity of such a black hole, which is probably determined by the availability of fuel in its vicinity and the efficiency of the accretion process, will determine whether the nucleus is classified as ‘active’ or ‘normal’. The division between these two classes is a matter of taste and our ability to detect very low levels of AGN activity.

A much more unclear picture is that of *small* galaxies, which constitute most galaxies by number, and a significant fraction of the stellar mass in the universe. The presence of massive black holes in non-active small galaxies has not been determined from dynamical evidence, except for a few exceptional cases such as NGC 221 (Bender, Kormendy & Dehnen 1996; van der Marel et al. 1997). Theoretical grounds are also sketchy, since small galaxies are expected to have undergone only a small number of merger events during their formation process and their black holes might only be at a ‘seed’ stage, if present at all.

AGN activity in small galaxies is therefore a very important test for galaxy evolution since it probes the presence of black holes in

Table 9. Summary of the inferred star formation history and abundances for our sample as a percentage of the inferred 4020-Å flux and mass. Targets have been sorted by a Hubble type and absolute magnitude. Also, the nuclear or off-nuclear location of the targets has been distinguished.

	Flux			Mass			Flux			Mass		
	(Y) (per cent)	(I) (per cent)	(O) (per cent)	(Y) (per cent)	(I) (per cent)	(O) (per cent)	(0.2 $Z_\odot$) (per cent)	($Z_\odot$) (per cent)	(2.5 $Z_\odot$) (per cent)	(0.2 $Z_\odot$) (per cent)	($Z_\odot$) (per cent)	(2.5 $Z_\odot$) (per cent)
E–S0 (19 per cent)	28.2	47.7	24.0	0.1	26.4	73.5	51.1	13.1	35.8	18.1	44.0	37.9
Sa–Sb (12 per cent)	15.0	17.5	67.5	0.0	1.6	98.4	18.7	5.8	5.4	0.1	86.9	13.0
Sc–Sd (33 per cent)	29.1	49.9	21.0	2.1	36.1	61.8	58.8	16.1	25.2	35.3	21.9	42.8
Sd–Irr (36 per cent)	52.2	25.4	22.4	7.4	23.3	69.4	57.3	3.7	9.0	42.3	23.3	34.4
$M > -14.5$ (12 per cent)	61.2	25.0	13.8	20.2	14.3	65.5	62.0	27.2	10.9	20.4	53.7	25.8
$-14.5 > M > -17.5$ (43 per cent)	35.6	41.0	23.3	0.7	30.8	68.5	61.0	7.8	31.2	45.8	22.3	31.9
$-17.5 > M > -20.0$ (33 per cent)	30.0	34.9	35.1	1.9	28.2	69.9	50.6	31.5	17.9	29.5	42.8	27.7
$M < -20.0$ (12 per cent)	15.5	42.4	42.0	0.0	9.1	90.9	50.6	31.5	17.9	29.5	42.8	27.7
Nuclear (41 per cent)	21.5	46.4	32.1	1.0	30.4	68.6	43.1	22.3	34.6	15.6	39.7	44.7
Off-nuclear (59 per cent)	44.4	30.0	25.7	5.0	21.7	73.3	57.9	19.6	22.4	40.3	30.7	29.0

Table 10. Derived oxygen abundances in solar units.

Source	Strong line	[O III] λ4363	Source	Strong line	[O III] λ4363
NGC 185-1	0.22[a]	—	NGC 3738-3	0.32	—
NGC 185-2	0.21	—	NGC 3738-4	0.23	—
NGC 185-3	—	—	NGC 3738-5	0.12	0.16
NGC 185-4	—	—	NGC 3738-6	0.16	—
NGC 205	—	—	NGC 4144-1	0.34	—
NGC 221	—	—	NGC 4144-2	0.15	0.14
NGC 224	—	—	NGC 4144-3	0.41	—
NGC 247	—	—	NGC 4150-1	0.24	—
NGC 404	0.33	—	NGC 4236-1	—	—
NGC 598	—	—	NGC 4236-2	0.75	—
IC 342-1	—	—	NGC 4236-3	1.13	—
IC 342-2	—	—	UGC 7321	0.22	—
NGC 1560	0.10	0.08	NGC 4605	0.37	—
NGC 2366-3	0.11	0.12	NGC 4736	0.25[a]	—
NGC 2366-4	0.07	0.07	NGC 4826-1	0.87	—
NGC 2366-5	0.07	0.07	NGC 4826-2	0.96	—
NGC 2403-1	—	—	NGC 4826-3	1.91	—
NGC 2403-2	—	—	NGC 5204-1	0.23	—
NGC 2976-1	0.57	—	NGC 5204-2	0.37[a]	—
NGC 2976-2	1.08	—	NGC 5238-1	0.12	—
UGC 6456-1	0.05	0.06	NGC 5238-2	0.18	—
UGC 6456-2	0.04	0.05	NGC 5457-1	>2.0	—
UGC 6456-3	0.07	—	NGC 5457-2	>2.0	—
UGC 6456-4	—	—	NGC 6503	0.44	—
NGC 3738-1	0.17	—	NGC 6946	—	—
NGC 3738-2	0.10	0.09			

[a]Uncertain values due to poor line flux determinations (see Table 6).

galaxies where dynamical evidence is lacking and, by determining the Eddington ratio, the rate at which they are currently growing.

In light of the spectral classification determined in Section 6, it is now possible to establish the demographics of AGN and their relationship with the parent galaxy distribution. Out of the 33 galaxies from the sample which have a spectral classification from this and other work (see references in Table 12), three have a stellar spectrum, 19 have star-forming nuclei, and two have Type 1 Seyfert nuclei. In Section 5.3, we find good evidence that of the six objects which classify as LINERs, four are driven by star-forming related processes, while only two could still be driven by photoionization, in which case the presence of a low-luminosity AGN is a reasonable assumption.

The number of all AGN (Seyferts and photoionized LINERs) is $4.0^{+3.2}_{-1.9}$ (using the 1σ single-sided confidence limits appropriate for low number counts; Gehrels 1986). Therefore the fraction of AGN in our sample is 12^{+9}_{-6} per cent.[2]

We want to compare this result with those obtained from surveys of more luminous galaxies, such as the one conducted on the Palomar sample by Ho et al. (1995). Out of 486 classified galaxies, Ho et al. (1997b) found 52 Seyfert nuclei, corresponding to ∼11 per cent. However, the number of LINER nuclei is even larger

[2]1σ single-sided confidence limits for all computed fractions have been obtained using Gehrels (1986) formulism.

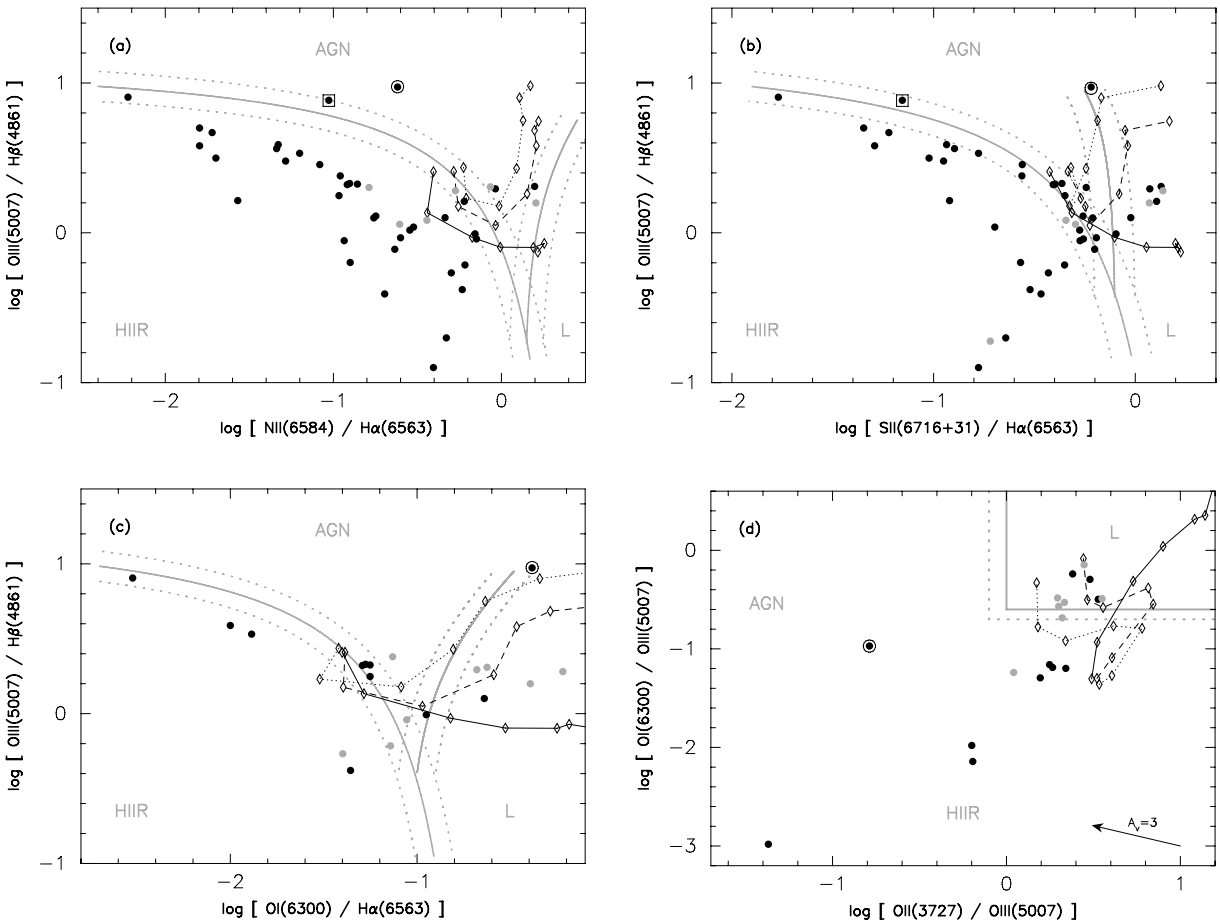

Figure 3. Diagnostic diagrams for emission-line spectra. The grey circles mark line ratios using lines with less-secure flux measurements (see Table 6). The theoretical division between the star-forming, AGN and LINER classes as parametrized by Kewley et al. (2001) is shown with a thick grey line in panels (a), (b), and (c). In panel (d) the line shows the LINER region using the criteria defined by Heckman etal. A reddening vector is also included. The dotted lines correspond to ± 0.1 dex from the lines dividing the spectral classes. Shock models from Allen et al. (2004) are included (◇). Each curve shows different line ratios corresponding to shock velocities of 100, 150, 200, 250, 300, 450 and 800 km s^{-1}, with velocities increasing towards the right-hand side of the panels. Different lines correspond to magnetic parameter $b = 1$ (continuous line), 5 (dashed line), and 10 (dotted line). See Allen et al. (2004) for more details. NGC 4395 and A 0951+68 have been labelled with a circle (○) and a square (□), respectively.

(94), and it is not clear which fraction are genuine AGN. Those showing a type 1 LINER nucleus (24) are clearly strong AGN candidates and therefore we can enlarge the number of total AGN to at least 76, implying a fraction of ∼16 per cent. Also, as mentioned in Section 6.1 recent studies using *Chandra* observations of optically classified LINERs find nuclear hard point-like sources in about 50–60 per cent of cases (Flohic et al. 2006; Gonzalez-Martin et al. 2006; Satyapal et al. 2006). These samples are dominated by luminous galaxies, and therefore these results are a good representation of the number of AGN-related LINERs in the Palomar sample, hence, increasing the fraction of AGN to ∼20–22 per cent. An upper limit to the AGN fraction can be adopted if all LINERs in the Palomar sample (94) are considered as AGN, implying a fraction of ∼33 per cent.

Table 11. Targets which fall in the LINER region of the diagnostic diagrams. The question marks show objects which fall within a 0.1 dex of the border that limits the LINER loci. The letters (a), (b), (c) and (d) refer to panels in Fig 3. See the text for further discussion on the AGN classification.

Galaxy	(Kewley et al. 2001)			(Heckman 1980)	AGN class
	(a)	(b)	(c)	(d)	
NGC 185		√	√	√	No
NGC 404		√	√	√	No
NGC 4150		√	√	√	Yes?
NGC 4736	√?	√	√	√	No
NGC 4826	√?	√	√	√	No
NGC 5457				√?	No
NGC 6503		√	√?	√	Yes?

It should be borne in mind that Ho et al. (1997b) also include 'Transition' nuclei in their AGN class (see Ho et al. 1997b for the definition of a Transition object), increasing their AGN fraction to ∼43 per cent. However, the nature of these objects is far from understood. In fact, out of the 65 Transition nuclei found in the Palomar sample, only two showed some evidence for broad wings, and of those objects with *Chandra* observations, very few seem to be consistent with the $L_{2-8\,\mathrm{keV}}$–$L_{\mathrm{H}\alpha}$ correlation determined from confirmed AGN (Ho et al. 2001).

The two confirmed AGN in our sample, NGC 3031 and NGC 4395, have Eddington ratios ∼10^{-5} and, ∼10^{-3}, respectively (Lira et al. 1999; Peterson et al. 2005; Lewis & Eracleous 2006), and both follow the M_{BH}–$\sigma^{\star}$ relation (Devereux et al. 2003; Greene & Ho 2006). We have derived Eddington ratios for the other two AGN candidates, NGC 4150 and NGC 6503, of $\lesssim 10^{-6}$, using the

Table 12. Nuclear spectroscopic classification. Spectral classes are: Sy = Seyfert, L = LINER, SF = star forming, A = starlight-dominated nucleus, SF-L = star-forming-driven LINER, and U = undetermined.

Galaxy	Class	Reference
NGC 147	U	1
NGC 185	SF-L	1
NGC 205	A	1,2,3
NGC 221	A	1,2,3
NGC 224	A	1,2,3
NGC 247	SF	1,3
NGC 253	SF	4
NGC 404	SF-L	1
NGC 598	SF	1
MAFFEI 1	U	1
MAFFEI 2	U	1
IC 342	SF	1,3
NGC 1560	SF	1,3
NGC 2366	U	1
NGC 2403	SF	3
NGC 2976	SF	1,3
A 0951+68	SF	5
NGC 3031	Sy	6,7
UGC 6456	SF	1
NGC 3738	SF	1,3
NGC 4136	SF	3
NGC 4144	SF	1,3
NGC 4150	L	1,3
NGC 4236	U	1
NGC 4244	SF	3
UGC 7321	SF	1
NGC 4395	Sy	3,8
NGC 4605	SF	1,3
NGC 4736	SF-L	1
NGC 4826	SF-L	1
NGC 5204	SF	1,3
NGC 5238	SF	1
NGC 5236	SF	3
NGC 5457	SF	1
NGC 6503	L	1
NGC 6946	SF	1,3
NGC 7793	SF	9

References. 1: this work; 2: Bica, Alloin & Schmidt (1990); 3: Ho et al. (1995); 4: Engelbracht et al. (1998); 5: Johnson et al. (1997); 6: Peimbert & Torres-Peimbert (1981a); 7: Ho et al. (1996); 8: Lira et al. (1999); 9: Diaz et al. (1982).

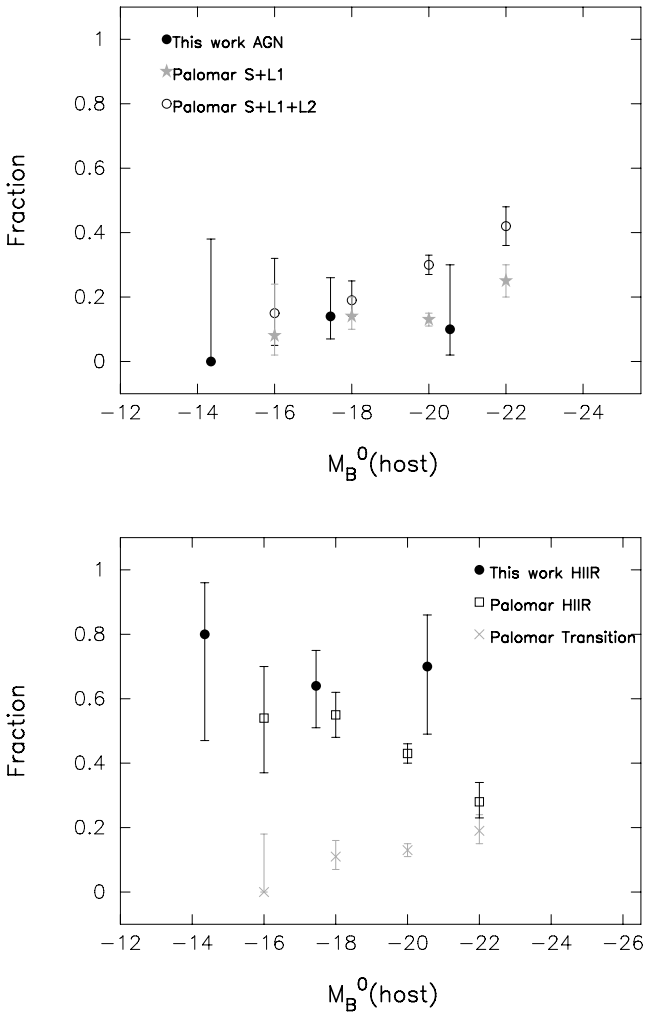

Figure 4. Top panel: fraction of AGN to total number of galaxies as a function of galaxy luminosity. Results come from the volume-limited sample (filled circles) and the Palomar sample of galaxies (empty circles for Seyferts and stars for LINER 1 nuclei). The error bars represent asymmetric 1σ confidence levels. Bottom panel: fraction of Transition and star-forming nuclei to total number of galaxies as a function of galaxy luminosity. Error bars are as before.

B bulge luminosities given by Ho et al. (1995) (after correcting for the different adopted distances to the galaxies), $B-R$ bulge colours measured from our own images, a 2–10 keV X-ray to bolometric luminosity ratio of 0.1, and a black hole mass–M_R relationship from Erwin, Graham & Caon (2004). These Eddington ratios, despite all the uncertainties involved, show that small galaxies in the local Universe, when active, seem to be extremely inefficient at fuelling their central black holes.

7.2 The luminosity-dependent fraction of AGN

We now study the characteristics of the galaxies that host the low-luminosity tail of the AGN population. The ratio of AGN to the total number of galaxies as a function of galaxy luminosity is shown in Fig. 4. Results from this work and from Ho et al. (1997b) for the Palomar sample are shown.

Both samples are nicely complementary. While Ho et al. (1997b) have a large number of galaxies with an absolute magnitude of $\lesssim -17$, we have extended the range of luminosities towards the very faint end, where distinguishing AGN from star-forming related activity becomes harder and each case has to be examined carefully. Since we have looked for evidence of AGN activity not only in obvious nuclear positions, but also in all potential knots in the central region of the galaxies in our sample, the results from our searching technique are very robust.

Fig. 4 shows a gentle increase in the fraction of active nuclei with host absolute magnitude spanning about four orders of magnitude. Since Ho et al. (1997b) do not distinguish between star-forming and AGN-related LINERs, we have computed the fraction of AGN with and without the contribution from type 2 LINERs (under the assumption that type 1 LINERs have a secure AGN classification) and show this in Fig. 4. Clearly, the sample that includes type 2 LINERs shows a very similar trend to that of 'secure AGN' (namely, Seyfert galaxies and type 1 LINERs), in agreement with a large

fraction of LINERs 2 being genuine AGN, as also shown by the *Chandra* results (Flohic et al. 2006; Gonzalez-Martin et al. 2006; Satyapal et al. 2006).

This trend – a positive correlation between activity and host luminosity – can be understood in the framework of the connection between black holes and their host galaxies. If the black hole mass systematically decreases with that of the spheroidal of their hosts, and ultimately with the size of the whole galaxy, then it is expected that the number of active nuclei might be systematically missed in low-luminosity galaxies, as the signs of activity fall below our detection threshold. Our finding that the Eddington ratios are particularly small in the AGN in our sample, reinforces this view. Furthermore, it is impossible at this stage to know whether black holes are also present in the smallest galaxies.

Ho et al. (1997b) also classify 'Transition' nuclei as AGN. 'Transition' nuclei from the Palomar sample are shown in the bottom panel of Fig. 4. Their behaviour is similar to that shown by Seyfert and type 1 LINER nuclei, also showing a slow rise in the fraction of nuclei with host luminosity.

As a comparison, galaxies classified as having a star-forming nuclei are also shown in the bottom panel of Fig. 4. The presence of star-forming nuclei clearly anticorrelates with host luminosity. This behaviour is well understood since dwarf galaxies are more prone to star-forming activity than massive galaxies. This very different behaviour shown by star-forming nuclei and those classified as Transition objects argues in favour of a distinctively different mechanism or physical condition to produce the observed characteristic in their spectra. In fact, Fig. 4 suggests a common behaviour for Seyfert, LINER and Transition nuclei.

Still, the detailed analysis of the galaxies performed in the previous sections has shown that not all LINERs have clear signs of being powered by an active nucleus. If a fraction is indeed powered by star-forming activity, how can we explain Fig. 4?

Metallicity could be in part responsible for the differences. In fact, Alonso-Herrero et al. (2000) found that the LINER spectral characteristics are well explained by aging star-forming regions where a metal-rich starburst and an SNR component are required to explain the optical spectra. This could explain the correlation between star-forming related LINER and Transition nuclei with host luminosity, since star-forming regions would show such spectral characteristics when harbour by more metal-rich, massive galaxies.

Alternatively, LINER and Transition nuclei without clear evidence for *ongoing* AGN activity, such as broad wings from a broad line region or the presence of a hard point X-ray source, could represent a dormant phase of the active nucleus, as has been suggested in the past for Seyfert 2 galaxies (see Lawrence 1987 and references therein). The large sizes of the NLR imply that this region would remain unchanged for hundreds or even thousand of years. This is much longer than the recombination time even for a low-density medium ($\sim 1/\alpha_{\rm A} n_{\rm H} \sim 12$ years from the moment the flux of ionizing photons stops, with $\alpha_{\rm A}$ the total hydrogen recombination coefficient, and $n_{\rm H} \sim 10^4$ cm^{-3} for an NLR). Therefore, it could be possible that the nebular emission is still present even though the signature of the central source is long gone.

8 SUMMARY

We have conducted a detailed imaging and spectroscopic study of a volume-limited sample of 37 galaxies in the Northern hemisphere. The spectra from the most-conspicuous knots of emission in the nuclear region of the galaxies were modelled using the STARLIGHT population-synthesis code to determine the properties of the underlying stellar populations. We found a broad range of ages for the studied regions, from populations dominated by stars with $t < 10^8$ yr to those where most of the stars have $t > 10^9$ yr.

Pure emission-line spectra were obtained after the subtraction of the modelled stellar component. Diagnostic diagrams were employed to separate the sources into star-forming, AGN and LINERs. Detail analysis of the LINER objects showed that most of them are more likely powered by star-formation activity.

Our volume-limited sample was combined with the Palomar sample studied by Ho et al. (1995) to study the trends in the fraction of AGN to total number of galaxies as a function of host galaxy luminosity. It was found that for $M_B \sim -12$ to -22 the AGN fraction presents a rising trend with host luminosity. This result is strengthen if all LINERs and 'Transition' nuclei from the Palomar sample are included. However, it is still an open question whether all such objects correspond to genuine AGN, in the sense that their output emission is primarily driven by an active nucleus.

ACKNOWLEDGMENTS

We are indebted to N. Vale Asari for performing the STARLIGHT fitting. PL is grateful of support by the Fondap project No 15010003. This research has made use of the NASA/IPAC Extragalactic Data base (NED) which is operated by the Jet Propulsion Laboratory, California Institute of Technology, under contract with the National Aeronautics and Space Administration.

REFERENCES

Allen M. G., Sutherland R., Dopita M. A., Kewley L. J., Groves B. A., 2004, in Storchi-Bergmann T., Ho L. C., Schmitt H. R., eds, IAU Symp. 222, The Interplay Among Black Holes, Stars and ISM in Galactic Nuclei. Cambridge Univ. Press, Cambridge, p. 305
Alonso-Herrero A., Rieke M. J., Rieke G. H., Shields J. C., 2000, ApJ, 530, 688
Baldwin J. A., Phillips M. M., Terlevich R. J., 1981, PASP, 93, 5
Barth A. J., Ho L. C., Filippenko A. V., Rix H.-W., Sargent W. L. W., 2001, ApJ, 546, 205
Becker R., White R., Helfand D., 1995, ApJ, 450, 559
Bender R., Kormendy J., Dehnen W., 1996, ApJ, 464, L123
Bica E., Alloin D., 1986, A&A, 162, 21
Bica E., Alloin D., Schmidt A. A., 1990, A&A, 228, 23
Bietenholz M., Bartel N., Rupen M., 2000, ApJ, 532, 895
Bietenholz M. F. et al., 1996, ApJ, 457, 604
Böker T. et al., 1999, ApJS, 124, 95
Böker T., Laine S., van der Marel R., Sarzi M., Rix H.-W., Ho L., Shields J., 2002, AJ, 123, 1389
Böker T., Forster-Schreiber N., Genzel R., 1997, AJ, 114, 1883
Bolatto A., Simon J., Leroy A., Blitz L., 2002, ApJ, 565, 238
Brinkman A. C., Kaastra J. S., van der Meer R. L. J., Kinkhabwala A., Behar E., Kahn S. M., Paerels F. B. S., Sako M., 2002, A&A, 396, 761
Bruzual G., Charlot S., 2003, MNRAS, 344, 1000
Buta R. J., McCall M. L., 1983, MNRAS, 205, 131
Cappellari M., Bertola F., Burstein D., Buson L., Greggio L. A. R., 1999, ApJ, 515, 17
Cardelli J. A., Clayton G. C., Mathis J. S., 1989, ApJ, 345, 245
Cid Fernandes R., Gu Q., Melnick J., Terlevich E., Terlevich R., Kunth D., Rodrigues Lacerda R., Joguet B., 2004, MNRAS, 355, 273
Cid Fernandes R., Mateus A., Sodré L., Stasińska G., Gomes J. M., 2005, MNRAS, 358, 363
Crane P., Dickel J., Cowan J., 1992, ApJ, 390, 9
Da Costa G., Mould J., 1988, ApJ, 334, 159
Davidge T. J., 2002, AJ, 124, 2012
Davidge T., 2005, AJ, 130, 2087
Davidge T., Courteau S., 2002, AJ, 123, 1438

del Burgo C., Mediavilla E., Arribas S., 2000, ApJ, 540, 741
Devereux N., Ford H. J. G., Jacoby G., 1997, ApJ, 481, L71
Devereux N., Ford H., Tsvetanov Z., Jacoby G., 2003, AJ, 125, 1226
Diaz A. I., Pagel B. E. J., Edmunds M. G., Phillips M. M., 1982, MNRAS, 201, 49P
Dopita M. A., Sutherland R. S., 1995, ApJ, 455, 468
Dopita M. A., Koratkar A. P., Allen M. G., Tsvetanov Z. I., Ford H. C., Bicknell G. V., Sutherland R. S., 1997, ApJ, 490, 202
Drissen L., Roy J.-R., Moffat A., Shara M., 1999, AJ, 117, 1249
Dubus G., Long K. S., Charles P. A., 1999, ApJ, 519, 135
Dudik R. P., Satyapal S., Gliozzi M., Sambruna R. M., 2005, ApJ, 620, 113
Elmegreen D., Chromey F., Warren A., 1998, AJ, 116, 2834
Engelbracht C. W., Rieke M. J., Rieke G. H., Kelly D. M., Achtermann J. M., 1998, ApJ, 505, 639
Eracleous M., Halpern J. P., 2001, ApJ, 554, 240
Eracleous M., Shields J. C., Chartas G., Moran E. C., 2002, ApJ, 565, 108
Erwin P., Graham A. W., Caon N., 2004, in Ho L. C., ed., Coevolution of Black Holes and Galaxies. Cambridge Univ. Press, Cambridge, p. 12
Ferguson H. C., Binggeli B., 1994, A&AR, 6, 67
Fingerhut R., McCall M., De Robertis M., Kingsburgh R., Komljenovic M., Lee H., Buta R., 2003, ApJ, 587, 672
Flohic H. M. L. G., Eracleous M., Chartas G., Shields J. C., Moran E. C., 2006, ApJ, 647, 140
Forbes D., Polehampton E., Stevens I., Brodie J., Ward M., 2000, MNRAS, 312, 689
Fraternali F., Cappi M., Sancisi R., Oosterloo T., 2002, ApJ, 578, 109
Freedman W. et al., 2001, ApJ, 553, 47
Galarza V. C., Walterbos R. A. M., Braun R., 1999, AJ, 118, 2775
Gallais P., Rouan D., Lacombe F., Tiphene D. I. V., 1991, A&A, 243, 309
Gallazzi A., Charlot S., Brinchmann J., White S. D. M., Tremonti C. A., 2005, MNRAS, 362, 41
Galliano E., Alloin D., Pantin E., Lagage P. O., Marco O., 2005, A&A, 438, 803
Gebhardt K. et al., 2001, AJ, 122, 2469
Gehrels N., 1986, ApJ, 303, 336
Goad M., Roberts T., Knigge C., Lira P., 2002, MNRAS, 335, 67
Gonzalez-Delgado R. M. et al., 1994, ApJ, 437, 239
Gonzalez-Martin O., Masegosa J., Marquez I., Guerrero M. A., Dultzin-Hacyan D., 2006, A&A, 460, 45
Gordon S., Duric N., Kirshner R., Goss W., Viallefond F., 1999, ApJS, 120, 247
Greene J. E., Ho L. C., 2006, ApJ, 641, L21
Greene J., Ho L., Ulvestad J., 2006, ApJ, 636, 56
Han M., Hoessel J., Gallagher J., Holtzmann J., Stetson P., 1997, AJ, 113, 1001
Harris J., Calzetti D., Gallagher J. III, Conselice C., Smith D., 2001, AJ, 122, 3046
Heckman T. M., 1980, A&A, 87, 152
Ho L., Ulvestad J., 2001, ApJS, 133, 77
Ho P., Beck S., Turner J., 1990, ApJ, 349, 57
Ho P., Turner J., Fazio G., Willner S., 1989, ApJ, 344, 135
Ho L. C., Filippenko A. V., Sargent W. L. W., 1995, ApJS, 98, 477
Ho L. C., Filippenko A. V., Sargent W. L. W., 1996, ApJ, 462, 183
Ho L. C., Filippenko A. V., Sargent W. L. W., 1997a, ApJS, 112, 315
Ho L. C., Filippenko A. V., Sargent W. L. W., 1997b, ApJ, 487, 568
Ho L., Schuyler D., Pooley G., Sramek R., Weiler K., 1999, AJ, 118, 843
Ho L. C. et al., 2001, ApJ, 549, L51
Ho L., Terashima Y., Ulvestad J., 2003, ApJ, 589, 783
Hodge P., 1976, AJ, 81, 25
Hummel E., van der Hulst J., Keel W., Kennicutt R., 1987, A&AS, 70, 517
Hunter D., Elmegreen B., van Woerden H., 2001, ApJ, 556, 773
Hurt R. L., Turner J. L., 1991, ApJ, 377, 434
Hurt R. L., Merrill K. M., Gatley I., Turner J. L., 1993, AJ, 105, 121
Iwasawa K., Fabian A. C., Almaini O., Lira P., Lawrence A., Hayashida K., Inoue H., 2000, MNRAS, 318, 879
Johnson R., Lawrence A., Terlevich R. D. C., 1997, MNRAS, 287, 333
Karachentsev I. D. et al., 2002, A&A, 383, 125
Karachentsev I. D. et al., 2003a, A&A, 398, 467
Karachentsev I. D. et al., 2003b, A&A, 398, 467
Karachentsev I. D. et al., 2003c, A&A, 404, 93
Karachentsev I. D., Sharina M. E., Dolphin A. E., Grebel E. K., 2003d, A&A, 408, 111
Karachentsev I. D., Karachentseva V., Huchtmeier W., Makarov D., 2004, AJ, 127, 2031
Kaspi S., Brandt W. N., Netzer H., Sambruna R., Chartas G., Garmire G. P., Nousek J. A., 2000, ApJ, 535, L17
Keel W. C., 1983, ApJS, 52, 229
Kewley L. J., Heisler C. A., Dopita M. A., Lumsden S., 2001, ApJS, 132, 37
Kim D.-C., Veilleux S., Sanders D. B., 1998, ApJ, 508, 627
Knapen J., Mazzuca L., Böker T., Shlosman I., Colina L., Combes F., Axon D., 2006, A&A, 448, 489
Kormendy J., McClure R., 1993, AJ, 105, 1793
Kraan-Korteweg R., 1986, A&AS, 66, 255
Kraan-Korteweg R., Tamman G., 1979, Astr. Nachr., 300, 181
Landolt A., 1983, AJ, 88, 439
Landolt A., 1992, AJ, 104, 340
Lauer T. et al., 1995, AJ, 110, 2622
Lauer T., Faber S., Ajhar E., Grillmair C., Scowen P., 1998, AJ, 116, 2263
Lawrence A., 1987, PASP, 99, 309
Lee M., Madore B., 1993, AJ, 106, 66
Lewis K. T., Eracleous M., 2006, ApJ, 642, 711
Lira P., Lawrence A., O'Brien P., Johnson R. A., Terlevich R., Bannister N., 1999, MNRAS, 305, 109
Lira P., Lawrence A., Johnson R. A., 2000, MNRAS, 319, 17 (Paper I)
Liu J.-F., Bregman J. N., 2005, ApJS, 157, 59
Mackey A. D., Gilmore G. F., 2003, MNRAS, 338, 120
Maddox L. A., Cowan J. J., Kilgard R. E., Lacey C. K., Prestwich A. H., Stockdale C. J., Wolfing E., 2006, AJ, 132, 310
Makarova L., Karachentsev I., 1998, A&AS, 133, 181
Maoz D., Filippenko A., Ho L., Rix H.-W., Bahcall J., Schneider D., Macchetto F., 1995, ApJ, 440, 91
Maoz D., Koratkar A., Shields J. C., Ho L. C., Filippenko A. V., Sternberg A., 1998, AJ, 116, 55
Martínez-Delgado D., Aparicio A., Gallart C., 1999, AJ, 118, 2229
Matthews L., Gallagher J., van Driel W., 1999, AJ, 118, 2751
McConnachie A., Irwin M., Ferguson A., Ibata R., Lewis G., Tanvir N., 2005, MNRAS, 356, 979
McKernan B., Yaqoob T., George I. M., Turner T. J., 2003, ApJ, 593, 142
Meier D., Turner J., 2001, ApJ, 551, 687
Méndez B., Davis M., Moustakas J., Newman J., Madore B., Freedman W., 2002, AJ, 124, 213
Minezaki T. et al., 2006, ApJ, 643, L5
Mohan N. R., Anantharamaiah K. R., Goss W. M., 2002, ApJ, 574, 701
Moody J., Roming P., Joner M., Hintz E., Geisler D., Durrell P., Scowen P., Jee R., 1995, AJ, 110, 2088
Moran E. C., Eracleous M., Leighly K. M., Chartas G., Filippenko A. V., Ho L. C., Blanco P. R., 2005, AJ, 129, 2108
Nagar N., Falcke H., Wilson A., Ho L., 2000, ApJ, 542, 186
Nagar N., Falcke H., Wilson A., Ulvestad J., 2002, A&A, 392, 53
Ogle P. M., Brookings T., Canizares C. R., Lee J. C., Marshall H. L., 2003, A&A, 402, 849
Pagel B. E. J., Simonson E. A., Terlevich R. J., Edmunds M. G., 1992, MNRAS, 255, 325
Peimbert M., Torres-Peimbert S., 1981a, ApJ, 245, 845
Peimbert M., Torres-Peimbert S., 1981b, ApJ, 245, 845
Peletier R., 1993, A&A, 271, 51
Pellegrini S., Fabbiano G., Trinchieri G., Antonelli A., 2002, A&A, 383, 1
Pellegrini S., 2005, ApJ, 624, 155
Pence W., Snowden S., Mukai K., Kuntz K., 2001, ApJ, 561, 189
Peterson B. M. et al., 2005, ApJ, 632, 799
Pilyugin L. S., 2000, A&A, 362, 325
Pogge R., Maoz D., Ho L., Eracleous M., 2000, ApJ, 532, 323
Ptak A., Colbert E., van der Marel R. P., Roye E., Heckman T., Towne B., 2006, ApJS, 166, 154
Rekola R., Jerjen H., Flynn C., 2005, A&A, 437, 823
Rickard L., Harvey P., 1983, ApJ, 218, 51

Rix H.-W., Kennicutt J. R., Braun R., Walterbos R., 1995, ApJ, 438, 155
Roberts T. P., Goad M. R., Ward M. J., Warwick R. S., O'Brien P. T., Lira P., Hands A. D. P., 2001, MNRAS, 325, L7
Roy J.-R., Aube M., McCall M. L., Dufour R. J., 1992, ApJ, 386, 498
Rubin V. C., Ford K. W. J., 1986, ApJ, 305, L35
Rubin V., 1994, AJ, 107, 173
Saha A., Claver J., Hoessel J., 2002, AJ, 124, 839
Sako M., Kahn S. M., Paerels F., Liedahl D. A., 2000, ApJ, 543, L115
Sambruna R. M., Netzer H., Kaspi S., Brandt W. N., Chartas G., Garmire G. P., Nousek J. A., Weaver K. A., 2001, ApJ, 546, L13
Sams B., Genzel R., Eckart A., Tacconi-Garman L., Hofmann R., 1994, ApJ, 430, 33
Satyapal S., Dudik R. P., O'Halloran B., Gliozzi M., 2006, ApJ, 642, 615
Satyapal S., Sambruna R. M., Dudik R. P., 2004, A&A, 414, 825
Schlegel D. J., Finkbeiner D. P., Davis M., 1998, ApJ, 500, 525
Schulte-Ladbeck R., Hopp U., Crone M., Greggio L., 1999, ApJ, 525, 709
Seth A., Dalcanton J., de Jong R., 2005, AJ, 130, 1574
Sharina M. E., Karachentsev I. D., Tikhonov N. A., 1997, Astron. Lett., 23, 373
Shuder J., Osterbrock D., 1981, ApJ, 250, 55
Skelton J. E., Lawrence A., Pappa A., Lira P., Almaini O., 2005, MNRAS, 358, 781
Taniguchi Y., Yoshino A., Ohyama Y., Nishiura S., 1999, ApJ, 514, 660
Terashima Y., Ho L. C., Ptak A. F., Mushotzky R. F., Serlemitsos P. J., Yaqoob T., Kunieda H., 2000, ApJ, 533, 729
Thim F., Tammann G., Saha A., Dolphin A., Sandage A., Tolstoy E., Labhardt L., 2003, ApJ, 590, 256
Thim F., Hoessel J., Saha A., Claver J., Dolphin A., Tammann G., 2004, AJ, 127, 2322
Tikhonov N. A., Galazutdinova O. A., Aparicio A., 2003, A&A, 401, 863
Turner J., Ho P., 1983, ApJ, 268, 79
Turner J., Ho P., 1985, ApJ, 299, 77
Turner J., Ho P., 1994, ApJ, 421, 122
Ulvestad J., Antonucci R., 1997, ApJ, 488, 621
Ulvestad J., Ho L., 2002, ApJ, 581, 925
Uson J., Matthews L., 2003, AJ, 125, 2455
van der Marel R. P., de Zeeuw P., Rix H.-W., Quinlan G. D., 1997, Nat, 385, 610
Veilleux S., Osterbrock D. E., 1987, ApJS, 63, 295
Walcher C. J., Böker T., Charlot S., Ho L. C., Rix H.-W., Rossa J., Shields J. C., van der Marel R. P., 2006, ApJ, 649, 692
Weaver K., Heckman T., Strickland D., Dahlem M., 2002, ApJ, 576, 19
White R. L., Becker R. H., Helfand D. J., Gregg M. D., 1997, ApJ, 475, 479
Wrobel J., Heeschen D., 1991, AJ, 101, 148
Wrobel J. M., Ho L. C., 2006a, ApJ, 646, L95
Wrobel J., Ho L., 2006b, ApJ, 646, 95
Wrobel J., Fassnacht C., Ho L., 2001, ApJ, 553, 23
Yaqoob T., McKernan B., Kraemer S. B., Crenshaw D. M., Gabel J. R., George I. M., Turner T. J., 2003, ApJ, 582, 105
Young L., Lo K., 1997, ApJ, 476, 127

APPENDIX A: NOTES ON INDIVIDUAL OBJECTS

(i) *NGC 147:* No obvious nucleus was found in this galaxy. Of the three prominent optical sources in the centre of this galaxy sources 1 and 2 are unresolved and show a stellar spectrum consistent with early F- and G-type stars, respectively. They would correspond to foreground stars located at a distance of ∼2 kpc. The third bright source corresponds to a globular cluster (Hodge 1976; Da Costa & Mould 1988; Han et al. 1997).

(ii) *NGC 185:* Spectra were obtained for four very red knots seen in the *J* band. Knot 1 is also coincident with a bright optical source, and the other three knots are close to regions of enhanced optical emission. With $M_V \sim -5$, the knots probably correspond to stellar clusters in NGC 185 or individual evolved stars (Davidge 2005). The other bright optical sources seen in the centre of this galaxy are a mixture of blue star clusters (Martínez-Delgado et al. 1999) and probably foreground stars. The cross in Fig. 2 marks the position of the 2-cm radio detection of Nagar et al. (2000). It is not consistent with an obvious source in any of the images.

(iii) *NGC 205 – M 110:* Bica et al. 1990 performed population synthesis of the nuclear spectra and inferred that the dominant stellar population has an age between 0.1 and 0.5 Gyr, with subsolar metallicities. This is in very good agreement with our population-synthesis results, except for the derived metallicities. A modest burst of star formation also took place ∼50–100 Myr ago (Peletier 1993; Cappellari et al. 1999).

(iv) *NGC 221 – M 32:* Spectral synthesis by Bica et al. (1990) shows that the nuclear spectra are dominated by an old (>10 Gyr) stellar population with solar metallicities, although an intermediate-age population (∼5 Gyr) is also significant. These values agree very well with our results.

(v) *NGC 224 – M 31:* The M31 nucleus is highly compact, and is the prototype of the central luminous star clusters found in many galaxies. The bulk of its stellar population corresponds to an old ($\gtrsim$10 Gyr) metal-rich component (Bica et al. 1990). This is also reproduced by our synthesis analysis. The central 1 kpc of M 31 contains several ionized gas clouds, which interestingly have different line ratios, placing them in the Seyfert, LINER or star-forming regions of line ratio diagrams (delBurgo et al. 2000).

(vi) *NGC 247:* The colours of the bright central sources are consistent with their being star-forming regions. Paα emission is also seen in the central regions (Böker et al. 1999). The nucleus of this galaxy appeared unresolved in the UV (Maoz et al. 1995). Our spectral analysis implies a combination of young, intermediate and old stars.

(vii) *NGC 253:* The star formation in this well-known starburst galaxy is dominated by the inner 200 pc region (Engelbracht et al. 1998), which is spatially complex, as can be seen in Fig. 2. The nucleus of the galaxy has been identified at radio and mid-IR wavelengths (Galliano et al. 2005). *HST* images show young star clusters in the centre that trace out a ≈50 pc ring (Forbes et al. 2000). Most of the compact radio sources lie inside this ring, and are not coincident with optical or NIR sources. The brightest radio source is likely the galaxy nucleus (Turner & Ho 1985; Ulvestad & Antonucci 1997). It is coincident with a weak NIR source (Sams et al. 1994). It is likely that the radio source marks the position of a low-luminosity AGN (Mohan & Anantharamaiah 2002). A highly obscured hard X-ray source is detected by *Chandra* at the radio source position (Weaver et al. 2002).

(viii) *NGC 404:* The blue colour of the nucleus and the circumnuclear regions are apparent in Fig. 2. The red dust patch to the north-east of the nucleus seen in the B/I image is also seen in the *HST* $V - I$ image of Pogge et al. (2000). *HST* observations at UV wavelengths of this galaxy show that its nucleus is dominated by stellar absorption features from massive young stars (Maoz et al. 1998). The starburst is also detected in the X-rays (Eracleous et al. 2002). Ho et al. (1995) classified this nucleus as a LINER and this classification is confirmed here (Section 7.3). The signature of a population of young stars is also clear in Fig. 2 and is confirmed by our spectral analysis.

(ix) *NGC 598 – M 33:* This Local Group galaxy has a stellar cluster like nucleus with a substantial colour gradient, the centre being bluer (Kormendy & McClure 1993; Lauer et al. 1998). The X-ray and radio sources coincident with the nucleus have properties very similar to those of high-state stellar black hole candidates found in our Galaxy (Dubus & Long 1999; Gordon et al. 1999). The mass of

any central black hole in NGC 598 is constrained to be $<1500\,M_\odot$ (et al. 2001). The peculiar [N II] λλ6548,6584–Hα features seen in Fig. 2, with [N II] in emission and Hα in sharp, deep absorption, have been already noted by Rubin & Ford (1986). Our spectral analysis shows that the nucleus underwent a strong starburst episode about 1 Gyr ago and has had little star-forming activity ever since.

(x) *MAFFEI 1:* A foreground extinction of $A_V = 4$–5 mag has been measured towards this galaxy (Buta & McCall 1983; Davidge 2002). Spectral observations were only obtained in the red, hence no spectral classification was possible. The extinction-corrected spectrum shows Hα in emission as well as strong absorption features and our spectral analysis confirms the presence of stellar populations with a wide age range.

(xi) *MAFFEI 2:* This spiral is also heavily obscured. The internal nuclear extinction has also been found to be large, with $A_V \gtrsim 10$ mag (Hurt & Turner 1991; Hurt et al. 1993). The nuclear region is the site of a vigorous burst of star formation, indicated by radio continuum emission (Turner & Ho 1994), strong infrared emission (Rickard & Harvey 1983; Ho et al. 1989), as well as NIR (Ho et al. 1990) and optical emission lines (Fig. 2). The nucleus of the galaxy is obvious in our NIR images. Five radio sources are found within a radius of ∼100 pc (see Table 2). Spectral observations were only obtained in the red; hence, no spectral classification was possible. Spectra were taken at the position of the brightest optical source and two radio sources (see Table 5). One of the radio sources (source 2) seems to be coincident with the IR peak while the other radio source (source 3) is coincident with an optical knot. The optical images clearly show the effects of dust extinction. These are much reduced in the *J*-band image, where we see a bright nuclear source that is not seen in the optical images.

(xii) *IC 342:* NIR and molecular gas observations show a young nuclear stellar cluster, a small-scale nuclear stellar bar, and a star-forming ring at the Inner Lindblad Resonance (ILR) of the bar with a radius of only 50 pc (Böker et al. 1997; Meier & Turner 2001). The nuclear star-forming ring is partially seen in our V/I image. A nuclear stellar cluster lies at the centre of the ring and is clearly seen in Fig. 2. In the optical we also see two bright blue regions to the north and south of the nucleus which are located within the stellar bar. The positions of the three central radio peaks marked in Fig. 2 were measured from the 6-cm map in fig. 1 of Turner & Ho (1983), as positions are not given in the paper. Spectra were acquired of the nucleus and the southern blue region. After correcting for foreground extinction, the spectra appear very blue. Our population-synthesis analysis shows that the nuclear stellar cluster is not older than 100 Myr and the blue southern region is only 1 Myr old. The Balmer decrement suggests significant intrinsic extinction. This is confirmed by IR observations (Böker et al. 1997).

(xiii) *NGC 1560:* Images of NGC1560 in Lee & Madore (1993) show that there is no obvious nucleus. A spectrum of the approximately central position shows a starburst nucleus with subsolar metallicities where a very recent ($\lesssim$ few Myr) burst of star formation took place.

(xiv) *NGC 2366:* Fig. 2 shows that there is no obvious nucleus in this galaxy. The only radio source is associated with the giant H II region NGC 2363 located in the south-west of the galaxy (Hunter et al. 2001). Spectra were acquired for two bright sources (labelled 1 and 2 in the figure) located in the north and central part of NGC 2366 and three sources located in the NGC 2363 region (labelled 3–5). Source 1 shows some emission lines superimposed on the characteristic undulating continuum of M-type stars. This spectrum corresponds to the observations obtained by Ho et al. (1995) who identified the target as a foreground star. The knot is, however, resolved in our images and probably corresponds to a stellar cluster. If located in NGC 2366, its absolute visual magnitude corresponds to −9.8, with a linear size of ∼30 pc. This is similar to the characteristics of NGC 2004, a young cluster in the Large Magellanic Cloud which is also dominated by the features of M giant stars (Bica & Alloin 1986; Mackey & Gilmore 2003). Source 2 is unresolved and probably corresponds to an early G-type foreground star. The large [O III] λ5007/Hβ ratio seen in sources 3–5 (Fig. 2) imply high-excitation conditions in all the star-forming regions. The giant H II region NGC 2363 has been studied by Roy et al. (1992). They have found that source 4 shows low-intensity broad wings in Hα, Hβ and [O III] λ5007 emission lines. Gonzalez-Delgado et al. (1994) also found broad emission lines at 4660 and 5810 Å attributed to Wolf–Rayet stars. A detail of the spectrum of this source can be seen in Fig. A1 where the broad wings and the Wolf–Rayet hump can be appreciated.

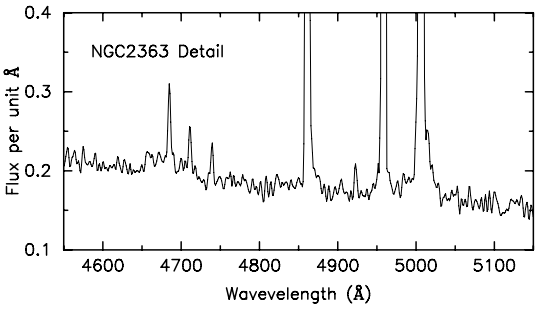

Figure A1. Detail of the NGC 2366-4 spectrum showing broad components in the oxygen lines and a hump at ∼4660 Å thought to be due to the presence of Wolf–Rayet stars.

(xv) *NGC 2403:* The nuclear cluster (labelled source 1) is apparent in Fig. 2. It is just resolved in our images and completely resolved in *HST* images (Drissen et al. 1999). The B/I image shows that the cluster is redder than the average colour of the cirumnuclear regions. The two bright knots to the east of the nucleus are found to be extended objects in the AO imaging of Davidge & Courteau (2002). They suggest that these objects could be blends of two or more stars, or compact star clusters. Spectra of the nucleus and one of the extended sources (source 2) were obtained and can be seen in Fig. 2. Both show absorption features and very weak nebular emission lines. Our spectral analysis shows that both sources present very similar star formation histories. No radio or point-like X-ray emission is observed at the nucleus position (Turner & Ho 1994; Fraternali et al. 2002).

(xvi) *NGC 2976:* Fig. 2 shows that the the central kiloparsec of this galaxy contains several bright sources, but no obvious nucleus. The colours of the majority of the sources are typical of star-forming regions and many of them are extended. Source 1 has somewhat redder colours than the others. Spectra were obtained for two sources. They show strong emission lines. Source 2 also shows the presence of a young underlying stellar population with strong blue continuum. The spectral analysis shows that an older population is also present.

(xvii) *A 0951+68:* This dwarf elliptical contains an off-centre starburst region. The spectra of the nucleus and the star-forming region have been reported by Johnson et al. (1997).

(xviii) *NGC 3031 – M81:* This is a well-known nearby Seyfert 1 nucleus (Peimbert & Torres-Peimbert 1981b; Shuder & Osterbrock 1981). The nucleus is very bright, and is unresolved in *HST* images, with an upper limit to its diameter of 0.73 pc (Devereux & Ford 1997). There is a nuclear variable radio source with a core-jet morphology (Bietenholz et al. 2000).

(xix) *UGC 6456:* This blue compact dwarf galaxy has a central blue star-forming region and a smooth red outer halo populated by old stars (Schulte-Ladbeck et al. 1999). It does not contain an obvious nucleus. The spectra of four bright optical knots were obtained for this galaxy, but only one showed enough stellar continuum for a spectral analysis. The results show a young starburst only a few Myr old. Fig. 2 shows what seems to be the most probable optical counterpart of the luminous X-ray source (Paper 1) located at the northern edge of the central region (Source 5), but no spectroscopic data were acquired for this object. Source 4 is unusual. The [O II]λ3727/[O III] λ5007 ratio is >10, indicating a very low ionization parameter. It also shows a weak broad component in Hα (2300 km s^{-1} full width, zero intensity) and possibly Hβ. The lack of [O III] λ5007 rules out the possibility of this source being an AGN, and the weak [N II] and [S II] lines exclude an SNR scenario. A visual inspection of the spectrum reveals no hint of the broad emission lines attributed to Wolf–Rayet stars.

(xx) *NGC 3738:* There is no obvious nucleus in this galaxy. The central regions contain several blue spots, most of which have colours of star-forming regions. Spectra for six of the central blue regions were obtained. Some beautiful examples of the Balmer series can be seen in several of the spectra.

(xxi) *NGC4136:* Fig. 1 shows the nuclear bar in this galaxy and the prominent nucleus. Nuclear spectra show strong nebular emission lines and weaker absorption (Ho et al. 1995).

(xxii) *NGC 4144:* There is no obvious nucleus in this galaxy. The spectrum of source 1 corresponds to the brightest knot seen in the optical images. The spectrum shows low-ionization emission lines and significant absorption features from a young population of stars. Source 3 corresponds to the brightest infrared peak and it is located approximately 1 arcsec to the east of source 1. The spectra of sources 1 and 3 are very similar. Source 2 corresponds to a high-excitation star-forming region located 4 arcsec north from source 1.

(xxiii) *NGC 4150:* Fig. 2 shows central structures in the B/I image, with a red nucleus consistent with the dust structures seen in the *HST* images (Lauer et al. 1995). The nuclear spectrum is dominated by absorption features with some weak emission lines. The X-ray source X1 in Paper I (source 2 in Fig. 2) has a position consistent with a knot of optical emission 15 arcsec away from the nucleus. Its spectrum reveals that it is in fact a background quasar at redshift 0.52. Its X-ray luminosity corresponds to 2–3 $\times$ 10^{44} erg s^{-1} in the 2–10 keV energy range (Appendix B).

(xxiv) *NGC 4236:* This galaxy does not contain an obvious nucleus. Spectra of three optical knots of emission were obtained for this galaxy. Source 1 is unresolved and it has spectrum consistent with a foreground late G-type star. Source 2 shows strong emission lines and clear evidence of absorption features from an underlying young stellar population. Source 3 corresponds to a relatively low-excitation star-forming region with near-solar abundances.

(xxv) *NGC4244:* Fig. 2 shows a prominent nucleus and a central dust lane. The nucleus of NGC4244 corresponds to a star-forming region (Ho et al. 1997a).

(xxvi) *UGC 7321:* This very edge-on galaxy has a very thin disc with no discernible bulge component (Matthews et al. 1999). The spectrum of this galaxy shows strong emission lines from a low-excitation star-forming region and absorption from a young underlying stellar population. The nebular emission gives a high upper limit for the abundances.

(xxvii) *NGC 4395:* The radio, IR, optical and X-ray characteristics of this galaxy have been extensively discussed by several authors (e.g. Lira et al. 1999; Iwasawa et al. 2000; Moran et al. 2005; Peterson et al. 2005; Skelton et al. 2005; Minezaki et al. 2006; Wrobel & Ho 2006a).

(xxviii) *NGC 4605:* The figure shows that the central nucleus is redder than its surroundings. We note also the asymmetry present in the disc in the large *R*-band image. The spectrum of the nucleus is dominated by emission lines and absorption features from a young stellar population.

(xxix) *NGC 4736 – M 94: HST* UV imaging of this galaxy shows two equally bright compact nuclear sources separated by 2.5 arcsec in the north–south direction (Maoz et al. 1995). The southernmost source corresponds to the nucleus and is also detected as a high brightness temperature compact radio source (Turner & Ho 1994) and in X-rays (Pellegrini et al. 2002). The nucleus of this galaxy is classified as a LINER and is a strong and complex X-ray source from point sources and extended emission (Paper I; Eracleous et al. 2002). The large B/I image in Fig. 2 shows a blue star-forming ring and associated radio emission from the FIRST survey. Red arcs are seen in the inner disc as well as a nuclear minibar (length $\approx$20 arcsec), which causes the central surface brightness contours to be elliptical. The colour structure in the nucleus of the galaxy is probably an artefact due to slightly different point spread functions (PSFs) in the two images.

(xxx) *NGC 4826:* The well-known large and clumpy dust lane on the northern side of the disc, which gives the galaxy its nickname 'Evil Eye', is clearly seen in our image. The FIRST radio map is overlaid on to the image. At higher resolution the central radio emission contains discrete components (Hummel et al. 1987; Turner & Ho 1994). Five sources are found within a radius of $\sim$100 pc (see Table 2); one of them coincident with the nucleus. Spectra were acquired for the nucleus and for two radio sources (see Table 5). The nuclear spectrum is dominated by absorption features with the presence of weak emission lines, while the radio sources (labelled 2 and 3) are dominated by nebular emission, although a clear stellar component is also present. The [S II]λλ6717,6730/Hα and [N II]λλ6548,6584/Hα for sources 2 and 3 indicate that they are both SNRs. Source 3 had been previously identified as a possible SNR by Rix et al. (1995).

(xxxi) *NGC 5204:* The *R* image in Fig. 2 shows a central, bright, slightly extended source (source 1) surrounded by a clumpy structure. Source 2 is the ultraluminous X-ray (ULX) source NGC5204-X1 (Roberts et al. 2001; Goad et al. 2002). A spectrum of source 1 was obtained and is dominated by emission lines with some strong absorption features from a young stellar population at the blue end. The [S II]/Hα and [N II]/Hα line ratios are not as strong as seen in an SNR. A spectrum of the ULX was also obtained. Despite the low S/N of the data, it is possible to appreciate several strong emission lines denoting the presence of a star-forming region. Roberts et al. (2001) also obtained an optical spectrum of this source through a fibre 0.9 arcsec in diameter, that is, of similar size to our slit aperture. [O III] λ5007 and Hα lines are seen in Roberts' spectrum. In our data, we also detect [S II]λλ6717,6730, [O III] λ5007 and [O II] λ3727, and after stellar subtraction, a weak Hβ feature. The continuum shape of the data obtained by Roberts et al. (2001) appears much bluer than ours and consistent with a very young ($<$10 Myr) stellar cluster. This disagreement might imply the acquisition of different targets by Roberts et al. (2001) and us.

(xxxii) *NGC 5238:* Fig. 2 shows a very clumpy central structure. There is no clear nucleus. The best candidate is source 1, which is marginally resolved. Spectra of this source and of another dimmer optical knot located $\sim$4 arcsec north from source 1 were obtained. Source 1 shows strong emission lines, evidence for an underlying

star population, and a very blue continuum. Source 2 corresponds to a pure star-forming region.

(xxxiii) *NGC 5236 – M 83:* Fig. 2 shows that the centre of this galaxy has complex structure in the optical and NIR (Gallais et al. 1991; Elmegreen et al. 1998). The radio emission from the central region is also complex, with multiple sources (Turner & Ho 1994; Harris et al. 2001; Maddox et al. 2006). The optical and NIR nucleus is coincident with the third brightest radio-peak (Maddox et al. 2006). NIR imaging (Elmegreen et al. 1998) shows two dust lanes going into the centre from opposite directions, and forming a circumnuclear ring in the centre. This ring is possibly joined to an inner ring by a nuclear bar. The main star-forming region is a partial arc lying between these two red rings and south of the nucleus. The crosses in Fig. 2 mark the 6-cm radio peaks from Turner & Ho (1994); however, there is also extended emission throughout the region. The radio peak positions are shifted slightly to correctly align the optical and radio sources (Gallais et al. 1991).

(xxxiv) *NGC 5457 – M 101:* Fig. 2 shows that the central region contains three bright sources, the northernmost of which corresponds to the nucleus (source 1). All the sources have Hα counterparts in the image of Moody et al. (1995). Dust features appear as light patches in the image of the central kiloparsec. X-ray observations with *Chandra* (Pence et al. 2001) show two nearly-identical nuclear X-ray sources coincident with the nucleus and source 2. There is a weak extended radio continuum source at the position of the nucleus (Turner & Ho 1994). Spectra were obtained for these two sources. The spectrum of the nucleus shows strong emission lines and absorption features from an underlying stellar population. Source 2 shows the spectrum of a reddened starburst region and a weak underlying stellar component. The very weak [O III] λ5007 line and strong [N II] and [S II] lines observed in both sources imply high metallicities.

(xxxv) *NGC 6503:* Fig. 2 shows a bright central nucleus. The nuclear spectrum shows prominent LINER emission lines and a red continuum with strong absorption features. *Chandra* observations show a very weak compact source coincident with the galaxy nucleus (Appendix B).

(xxxvi) *NGC 6946:* Fig. 2 shows a bright central nucleus. The central regions are affected by dust extinction (Elmegreen et al. 1998). There is radio emission coincident with the nucleus (Turner & Ho 1983). Strong emission lines can be appreciated in the nuclear spectrum. The steep red continuum and the large Balmer decrement denotes the strong extinction that affects the region. Despite the large [N II]$\lambda\lambda$6548,6584/Hα ratio, the observed strength of the [S II] lines is not enough to imply a significant contribution from SNRs. The weak oxygen emission lines but large [S II]/Hα and [N II]/Hα line ratios imply high metallicities. The non-detection of the [O II]λ3727 line prevents an estimation of the abundances.

(xxxvii) *NGC 7793:* This low-luminosity galaxy contains a nuclear stellar cluster (Böker et al. 2002). Optical nuclear spectra show the presence of a weak nuclear starburst (Diaz et al. 1982; Walcher et al. 2006).

APPENDIX B: *CHANDRA* OBSERVATIONS OF NGC 4150 AND NGC 6503

X-ray observations of NGC 4150 and NGC 6503 were obtained on 2000 October 29 and 2000 March 23 using the ACIS camera onboard the *Chandra* satellite. The total exposure time was 1.7 and 13.2 ks, respectively. The data reduction was done using CIAO software and the latest calibration files. The spectral analysis was limited to the 0.3–10 keV energy range.

Two and six compact sources with a detection significance larger than 5 were found to be associated with NGC 4150 and NGC 6503, respectively. A PSF analysis showed no significant deviations from point source profiles for any of them. Their coordinates are given in Table B1 and Fig. B1 shows a smoothed version of the X-ray data overlaid on to *R*-band images of the central region of both galaxies. Source b in NGC 4150 has already been identified as a background QSO (Appendix A). Source a in NGC 6503 is located farther away from the nuclear region and it is not shown in Fig. B1. Note that our *ROSAT* images in Paper I did not resolve any of the multiple nuclear sources shown here.

For both sources in NGC 4150 and the three brightest sources in NGC 6503 (a, d and f), we performed spectral analysis of the background-subtracted counts assuming an absorbed power-law model. The results are presented in Table B1.

The spectral fit to source a in NGC 4150 shows that a Galactic $N_{\rm H}$ column (1.6×10^{20} cm^{-2}) gives an acceptable fit. Letting

Table B1. Identification and results from spectral fitting and hardness-ratio analysis of the point sources in NGC 4150 and NGC 6503.

Source		Coordinates (J2000)		$N_{\rm H}$ (10^{20} cm^{-2})	Γ	$\chi^2_{\rm red}$	Count rate (2–10 keV)	Flux (2–10 keV) (erg s^{-1} cm^{-2})	Luminosity (2–10 keV) (erg s^{-1})	Notes
NGC 4150	a	12:10:33.8	30:23:58.2	1.6[a]	$1.31^{+.24}_{-.23}$	0.53	0.0092	2.1×10^{-13}	5.3×10^{39}	
	b	12:10:34.8	30:23:58.4	1.6	$1.65^{+.16}_{-.16}$	0.74	0.0098	2.4×10^{-13}	2.6×10^{44}	QSO at z = 0.52
				$5.7^{+3.0}_{-2.2}$	1.5	0.32		1.5×10^{-13}	1.8×10^{44}	
NGC 6503	a	17:49:12.5	70:09:31.3	4.1[a]	$1.51^{+.13}_{-.13}$	1.24	0.0014	5.4×10^{-14}	1.8×10^{38}	
	a			$22.8^{+9.7}_{-8.0}$	$2.39^{+.47}_{-.39}$	0.29		3.2×10^{-14}	1.1×10^{38}	
	b	17:49:26.5	70:08:39.8	10	1.5	–	0.0003	6.7×10^{-15}	2.2×10^{37}	Nuclear source
	c	17:49:27.9	70:08:36.9	10	1.5	–	0.0008	1.8×10^{-14}	6.0×10^{37}	
	d	17:49:28.8	70:08:32.9	4.1	$1.16^{+.12}_{-.12}$	1.17	0.0036	9.4×10^{-14}	3.1×10^{38}	
	d			$16.1^{+8.7}_{-6.9}$	$1.57^{+.29}_{-.26}$	0.85		7.7×10^{-14}	2.6×10^{38}	
	e	17:49:29.1	70:08:44.2	10	1.5	–	0.0007	1.4×10^{-14}	4.7×10^{37}	
	f	17:49:31.7	70:08:20.4	$60.0^{+12.4}_{-10.5}$	$2.20^{+.29}_{-.26}$	0.96	0.0073	1.2×10^{-13}	4.3×10^{38}	

[a]Galactic hydrogen column.

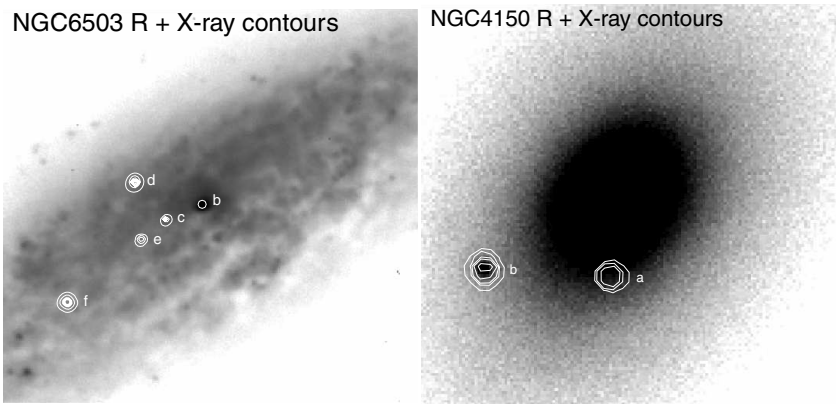

Figure B1. *R*-band 2 × 2 kpc and 3 × 3 kpc images of the central regions in NGC 4150 and NGC 6503, respectively, with overlaid X-ray contours.

$N_{\rm H}$ vary but freezing $\Gamma = 1.5$ resulted in a larger absorbing column. The 2–10 keV luminosity of this source puts it in the category of ULX sources (Liu & Bregman 2005; Ptak et al. 2006).

The spectral fit to the three brightest sources in NGC 6503 gives better statistical results when $N_{\rm H}$ is allowed to vary above the Galactic value (4.1×10^{20} cm^{-2}), consistent with the presence of absorbed, bright X-ray binaries. In fact, the best-fitting result for source 4 assuming a Galactic absorption column only was not acceptable ($\chi^2_{\rm red} = 3.8$).

For the three weakest sources in NGC 6503 (b, c and e), we performed a hardness ratio analysis. The results were consistent with a $\Gamma \sim 1.5$ and significant intrinsic absorption. Therefore, fluxes were derived assuming $\Gamma = 1.5$ and $N_{\rm H} = 1 \times 10^{21}$ cm^{-2}. The results are also presented in Table B1.

We find an upper limit of 4×10^{38} erg s^{-1} for a nuclear source in NGC 4150 in the 2–10 keV energy band. Source b in NGC 6503, with a luminosity of 8.0×10^{37} erg s^{-1} in the 2–10 keV energy band, is coincident with the galaxy nucleus. Satyapal et al. (2004) also reported on the detection of a nuclear source. However, based on the quoted number counts, we conclude that source c was misidentified as the galaxy nucleus. Our identification of source b as the nucleus is based on four-field X-ray point sources (most probably background QSOs) which have optical counterparts.

This paper has been typeset from a TEX/LATEX file prepared by the author.